Stochastic Simulation of Spin-1 Bosons at Ultra-Cold Temperatures

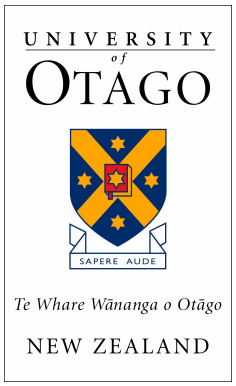

Author:
Steven Cromb

Supervisor:
Blair Blakie

Physics Department
University of Otago
Dunedin
New Zealand

19 September, 2014

A dissertation submitted in partial fulfilment of the requirements for the degree of BSc(Hons) in Physics

Abstract

Optical confinement of particles in 1998 allowed all hyperfine spin levels of a boson to be trapped and condensed in one system. Since this year the properties of these spin gases have opened new areas of exploration for theorists and experimentalists alike. In this dissertation I take new code designed to simulate the evolution of ultra-cold, spin-1 gases and test and validate it against information already known about spin-1 condensate systems. I then go on to demonstrate ways of applying the code to simulate experimental results and obtain a qualitative agreement with one particular experiment in doing so.

Acknowledgments

I would first like to thank the Physics Department at the University of Otago for giving me this opportunity to do research and explore areas of physics I would not have been able to through papers alone. The highs of achieving success and fun I have had during my research this year have been awesome.

I would also like to thank my parents. They let me live at home this year so I didn't have to worry about money and could focus on the project at hand. They also supported and encouraged me all the way.

To my classmates, thanks for the memories, may there be many more to come.

I'd like to thank the group that studies these systems along with me, each person has had some insight and helped me out even if in just a small way. Danny, Luke, Edward, Lewis and Ashton, thanks for your help.

And I'd like to make special mention to my supervisor Blair. He took me on as an honours student and did more than just have me do research, he got me excited about the research I was doing. In among everything else he does he has always been able to offer advice, help on interpreting results and probably the best thing was how he could show excitement at just the prospect of results. I have learned a lot from him, but none more than to enjoy the research you do. Thank you Blair.

Contents

Chapter 1

Introduction

A brief overview of the particles and system I am simulating and the reasons for wanting to do research in this area.

1.1 Bosons

A boson is any particle or composite particle (e.g. atom, molecule) with an integer amount of spin (f = 0,1,2...). These obey Bose statistics and any number of identical bosons can occupy the same single particle state at the same time. The multiple occupation of a single particle state is rare at temperatures in everyday life as usually there are too many high energy states to choose from for the number of particles in question (i.e. there is low phase/momentum space density). However when a gas of identical bosons is cooled to ultra-cold temperatures (typically in the realm of nanokelvins) the number of possible states to choose from decreases dramatically. When the temperature drops below a specific critical temperature there are significantly more bosons than accessible states many bosons will enter the lowest energy single particle state (i.e. the ground state). In doing so the individual particle wave-functions combine and acquire an identical phase, breaking U(1) symmetry and causing the onset of a state of matter known as Bose-Einstein Condensation.

1.2 Spin-1

I am simulating the evolution of spin-1 bosons. When the spin of a particle along an axis is measured it can take on any value from $+f$ to $-f$ in integer steps. So for a spin-1 boson a measured value can take 1, 0 or -1 as its result. These are the hyperfine spin levels of the boson. The matrix operators that measure the spin of a spin-1 boson are given by the following spin-1 matrices,

$$f_x = \frac{1}{\sqrt{2}} \begin{pmatrix} 0 & 1 & 0 \\ 1 & 0 & 1 \\ 0 & 1 & 0 \end{pmatrix}, \quad f_y = \frac{i}{\sqrt{2}} \begin{pmatrix} 0 & -1 & 0 \\ 1 & 0 & -1 \\ 0 & 1 & 0 \end{pmatrix}, \quad f_z = \begin{pmatrix} 1 & 0 & 0 \\ 0 & 0 & 0 \\ 0 & 0 & -1 \end{pmatrix}, \tag{1.1}$$

where the spin is measured in the x, y and z axes respectively for the normalised spinor of a boson, ζ, quantized in the z axis,

$$\zeta = \begin{pmatrix} \zeta_{+1} \\ \zeta_0 \\ \zeta_{-1} \end{pmatrix}_z, \quad \zeta^*\zeta = 1. \tag{1.2}$$

The spin of a particle gives it a magnetic moment which can be affected by a magnetic field. In the absence of a magnetic field the three spin levels along an axis are degenerate in terms of their energy, but with a magnetic field the energies of the spin levels can be shifted. This can cause changes in the way the one or many particles behave.

1.3 Spin-1 Condensation

Bose and Einstein first predicted the phenomenon of a macroscopic number of identical bosons falling to their ground state at low temperatures approaching absolute zero in 1924-5 [1, 2]. It was not until Anderson et al. [3] in 1995 that a Bose-Einstein Condensate (BEC) was first realised at JILA using a magnetic trap. Because of the magnetic nature of the trap only one spin state of the bosons could be trapped, with any others either being unaffected or repulsed by the trap. In 1998, Stamper-Kurn et al. [4] succeeded in trapping several million ultra-cold, spin-1 ^{23}Na bosons in an optical trap. The optical trap was able to trap all the hyperfine spin states of the boson equally meaning there could be spin degrees of freedom within the system and a spinor BEC was realised. To date ^{87}Rb is the only other spin-1 boson

to have been condensed [5]. Many experiments since [6–10] have demonstrated novel effects of the spin-1 BEC, such as spontaneous magnetisation causing axial symmetry breaking and domain formation, while theory has been developed [11–16] to describe the evolution of a spinor condensate and its low energy excitations.

1.4 Research Area and Motivation

While much research has been done on the zero temperature equilibrium dynamics of spin-1 bosons there is little theory for the influence of thermal effects on the condensate and its dynamics. The spin dependent energy (causing spin/magnetic ordering) is typically of the order of $\sim 1\,\mathrm{nK}$, while the coldest spinor BEC that has been achieved is $\approx 10\,\mathrm{nK}$ and in most of the experiments I have read about it is $\approx 50\,\mathrm{nK}$ which suggests thermal effects are significant in the evolution of spin-1 bosons in condensate experiments. Experiments have also explicitly cooled a system through the critical temperature for condensation meaning initially the system is completely thermal and has significant influence on the evolution of the condensate as it grows. These facts have motivated my research as I attempt to develop previously created code to a level where it can simulate similar effects to experimental results and be used at higher temperatures, up to the critical temperature for condensation, to predict the behaviour of spin-1 bosons above zero temperature.

Chapter 2

Spin-1 Classical Field Theory

In this chapter I discuss and develop the theory of spin-1 bosons to reach the equation governing their evolution, the Spin-1 Gross-Pitaevskii Equation (S1-GPE). I then go on to discuss the implications of the S1-GPE and introduce different versions of it, namely the reduction to a 2D dimensionless equation and the inclusion of damping and noise terms for the purpose of simulating finite temperature dynamics.

2.1 Evolution of Zero Temperature Spin-1 Bosons

2.1.1 Single Particle Evolution

The evolution of a single boson is governed, as with any particle[1], by the Schrödinger equation,

$$i\hbar\frac{\partial\Psi(\mathbf{x},t)}{\partial t} = \left(-\frac{\hbar^2\nabla^2}{2M} + V(\mathbf{x})\right)\Psi. \tag{2.1}$$

In the case of the spin-1 boson we consider the wave-function to be a three component complex vector field of spatial wave-functions (c.f. equation 1.2),

$$\Psi(\mathbf{x},t) = \begin{pmatrix} \psi_{+1} & (\mathbf{x},t) \\ \psi_0 & (\mathbf{x},t) \\ \psi_{-1} & (\mathbf{x},t) \end{pmatrix}, \tag{2.2}$$

[1]Ignoring massless and other relativistic particles

representing the three separate hyperfine spin states in the z axis and we take the trapping potential, $V(\mathbf{x})$, to be spatially dependent only, so it has no dependence on spin as expected of the optical traps described in section 1.3. The effect a magnetic field has on spin causes the potential for different spin levels to be Zeeman shifted by a magnetic field through the system. I consider a magnetic field along the z axis. At low magnetic fields there are two significant Zeeman energy shifts, the linear Zeeman energy, p, which shifts the energy levels proportional to the hyperfine spin of the particle along the field axis, and the quadratic Zeeman energy, q, which shifts the energy levels proportional to the square of the hyperfine spin of the particle along the magnetisation axis. These effects are shown visually in Figure 2.1. These

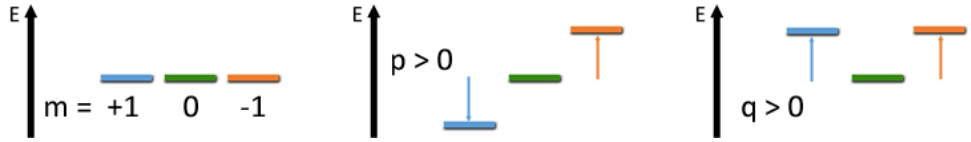

(a) No shift (b) Linear (c) Quadratic

Figure 2.1: The energies of the hyperfine spin levels are shifted under the influence of a magnetic field. These energy shifts can be separated into two types, linear shifts (b) and quadratic shifts (c)

shifts compete with interaction effects and can change the behaviour of the system dramatically in ways that will be discussed more later. Including Zeeman terms in the Schrödinger equation for the single particle dynamics gives,

$$i\hbar\frac{\partial\psi_m(\mathbf{x},t)}{\partial t} = \left(-\frac{\hbar^2\nabla^2}{2M} + V(\mathbf{x}) - pm + qm^2\right)\psi_m, \quad (m = 1, 0, -1), \quad (2.3)$$

where ψ_m is the m-component of the spin vector. This is the complete single particle equation of motion for a spin-1 boson. Because bosons can share the same single particle state, they can share the same wave-function. The vector field, Ψ, is the classical field; it represents all of the low energy bosons in the field with a total density given by normalising the wave-function to the density of the system,

$$\Psi^*\Psi = \begin{pmatrix} \psi_{+1}^* & \psi_0^* & \psi_{-1}^* \end{pmatrix} \begin{pmatrix} \psi_{+1} \\ \psi_0 \\ \psi_{-1} \end{pmatrix} = n(\mathbf{x}). \quad (2.4)$$

Table 2.1: The scattering lengths for spin-1 ^{23}Na and ^{87}Rb are given in units of the Bohr radius ($a_B = 0.0529$nm). Values taken from [15].

Atom	$F = 0$ scattering length (a_B)	$F = 2$ scattering length (a_B)
^{87}Rb	$a_0 = 101.8 \pm 0.2$	$a_2 = 100.4 \pm 0.1$
^{23}Na	$a_0 = 47.36 \pm 0.80$	$a_2 = 52.98 \pm 0.40$

However it now becomes necessary to include the effects of interactions between the bosons.

2.1.2 Spin Interactions

In BEC work only dilute gases are generally considered meaning only two body interactions are significant. At low energies these interactions can be approximated as an energy independent contact interaction[2] determined by the s-wave scattering length. When considering the collision of two identical particles with spin f, the total spin of the collision, F, can take on any value from zero to $2f$ in integer steps and is conserved is the collision process. For bosons F is restricted to even values due to symmetry considerations [15]. For the case of considering spin-1 bosons this means the possible total spins in a collision can be 0 or 2 and the only allowed collisions for which there is a change in the hyperfine spin populations is between two $m = 0$ bosons to produce one each of $m = \pm 1$ or the time reversed of this process. For all other collisions hyperfine spin population is conserved. $F = 0$ or $F = 2$ collisions each have their own scattering length; the scattering lengths of ^{87}Rb and ^{23}Na are given in table 2.1. The difference between the $F = 2$ and the $F = 0$ scattering lengths is of particular importance to the system and is discussed later in this chapter.

[2]Both ^{23}Na and ^{87}Rb have long range dipolar interactions, but these are far smaller than the contact interactions. They are not considered here but have been considered in experiment [17] and appear to influence evolution in specific circumstances (see appendix B).

The pseudo-potential for a collision of total spin F is proportional to an effective coupling constant, g_F, related to the scattering length as follows,

$$g_F = \frac{4\pi\hbar^2}{M} a_F. \tag{2.5}$$

It can be shown [11] that the effect of the interactions can then be incorporated by augmenting the Schrödinger equation with two interaction terms,

$$\begin{aligned} g_n n\psi_m, \quad &\rightarrow \quad g_n = \tfrac{g_0+2g_2}{3}, \\ g_s \textstyle\sum_{m'=-1}^{m} \mathbf{F}\cdot\mathbf{f}_{mm'}\psi_{m'}, \quad &\rightarrow \quad g_s = \tfrac{g_2-g_0}{3}, \end{aligned} \tag{2.6}$$

where g_n and g_s are known as the density and spin interaction terms respectively, $n = n(\mathbf{x})$ is the total number density and $\mathbf{F}$ is the spin density given by,

$$\mathbf{F}(\mathbf{x}) = \begin{pmatrix} F_x(\mathbf{x}) \\ F_y(\mathbf{x}) \\ F_z(\mathbf{x}) \end{pmatrix}, \quad F_\nu = \begin{pmatrix} \psi_{+1}^* & \psi_0^* & \psi_{-1}^* \end{pmatrix} f_\nu \begin{pmatrix} \psi_{+1} \\ \psi_0 \\ \psi_{-1} \end{pmatrix} \tag{2.7}$$

which takes the dot product with $\mathbf{f}_{mm'}$ to account for the allowed collisions; $\mathbf{f}_{mm'}$ is a vector of the mm' component of each of the spin-1 matrices (c.f. equation 1.1),

$$\mathbf{f}_{mm'} = \begin{pmatrix} f_{x_{mm'}} \\ f_{y_{mm'}} \\ f_{z_{mm'}} \end{pmatrix} \tag{2.8}$$

The density term, g_n, must be nonnegative to avoid collapse of the condensate system, but g_s, being proportional to the difference in the scattering lengths, can be positive or negative indicating that the boson in question favours antiferromagnetic or ferromagnetic interactions respectively. This selection leads to different sets of ground states available to the system and highlights g_s as one of the most significant factors in the spin-1 system.

With the interaction terms as the second addition to the Schrödinger equation the Spin-1 Gross-Pitaevskii Equation (S1-GPE) for a system of interacting spin-1 bosons is given as follows,

$$\begin{aligned} i\hbar\frac{\partial\psi_m(\mathbf{x},t)}{\partial t} = &\left(-\frac{\hbar^2\nabla^2}{2M} + V(\mathbf{x}) - pm + qm^2 \right)\psi_m \\ &+ g_n n\psi_m + g_s \sum_{m'=-1}^{m} \mathbf{F}\cdot\mathbf{f}_{mm'}\psi_{m'}, \quad (m = 1, 0, -1). \end{aligned} \tag{2.9}$$

2.1.3 Ground States of the Homogeneous S1-GPE

Consider the ground states of the S1-GPE for a homogeneous ($V = 0$) system with fixed density, n_0. The wave-function solution is assumed to be proportional to the spatially independent normalized spinor,

$$\begin{pmatrix} \psi_1 \\ \psi_0 \\ \psi_{-1} \end{pmatrix} = \sqrt{n_0} \begin{pmatrix} \zeta_1 \\ \zeta_0 \\ \zeta_{-1} \end{pmatrix}, \tag{2.10}$$

and the stationary states of the system are found. The ground state is then found to be the solution that minimizes the energy per particle,

$$\epsilon = \sum_{m=-1}^{1} (-pm + qm^2)|\zeta_m|^2 + \frac{1}{2}g_n n + \frac{1}{2}g_s n|\boldsymbol{f}|^2, \tag{2.11}$$

where,

$$\boldsymbol{f} = \frac{\mathbf{F}}{n}, \tag{2.12}$$

is the spin expectation value per particle. This analysis produces five different stationary state magnetic phases each with their own unique properties. The state with the lowest energy is determined by the sign of g_s and the ratios of p and q to $g_s n$, giving five different phases available to the spin-1 GPE as shown in Figure 2.2. Three phases are available to both a positive and negative g_s and correspond to a ground state with all the bosons in a single hyperfine spin level, $m = \pm 1$, known as the ferromagnetic ground states ($\zeta = (e^{i\chi}, 0, 0)^T$ or $\zeta = (0, 0, e^{i\chi})^T$, where χ is an arbitrary phase factor), or $m = 0$, known as the polar state ($\zeta = (0, e^{i\chi}, 0)^T$). Because they only have occupation in a single hyperfine spin level these states exhibit similar behaviour to a BEC with no spin interactions and no further symmetry additional to the U(1) symmetry has been broken. If g_s is greater than zero (i.e. $a_2 > a_0$, such as for ^{23}Na) then the boson has antiferromagnetic interactions, favours a minimised spin density and the Anti-Ferromagnetic (AF) phase appears. This phase occurs for $q < 0$ and $|p| < g_s n$ and has a population mixed between the $m = \pm 1$ states, with the density ratio, $|\zeta_{+1}|^2 : |\zeta_{-1}|^2$, changing continuously in linear fashion from $0:1$ to $1:0$ as p shifts from $-g_s n$ to $g_s n$. If g_s is less than zero (i.e. $a_2 < a_0$, such as for ^{87}Rb) then the boson has ferromagnetic interactions, favours a maximised spin density and a different phase appears known as the Broken Axis (BA)

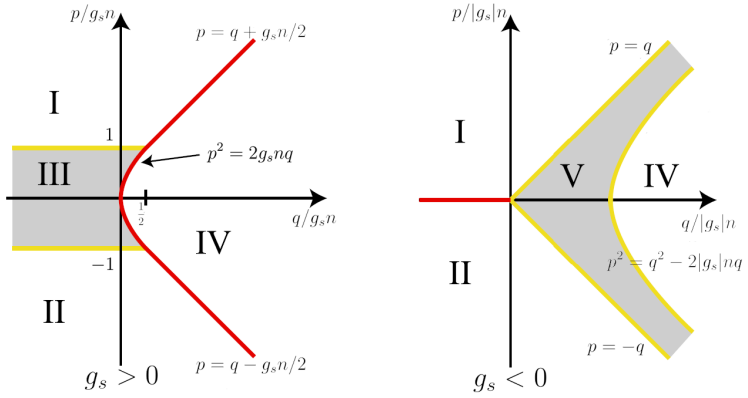

Figure 2.2: Phase diagrams of spin-1 Bose-Einstein condensates for (a) $g_s > 0$ and (b) $g_s < 0$. Regions I, II are the Ferromagnetic phases and IV is the Polar phase. The SO(2) rotational symmetry about the magnetic field is broken in the shaded regions, with III known as the Anti-Ferromagnetic phase and V known as the Broken-Axis phase. Figure adapted from [15]

phase. The BA phase occurs for values of q greater than $|p|$ in a region shown in Figure 2.2. It has population spread over all three hyperfine spin states and is dependent on both the linear and quadratic Zeeman. The AF and BA phases are of particular interest in spinor systems as they break axial symmetry, SO(2), around the z-axis of magnetisation. This is most obvious in the BA phase as the magnetic alignment of the spin tilts away from the z-axis of the magnetic field causing anisotropic magnetisation in the xy-plane. In the AF phase this symmetry is broken by the tensor density becoming anisotropic in the xy-plane [15] but magnetisation stays aligned with the z-axis.

2.2 Different Forms of the S1-GPE

2.2.1 Reduction to Two-Dimensions

Spin-1 experimental systems can be constructed in a way that is considered to be quasi-2D by increasing the trap frequency, ω, of one of the axes. The

main criteria to be quasi-2D is that the characteristic length,

$$l_\nu = \sqrt{\hbar/M\omega_\nu}, \quad (\nu = x, y, z) \tag{2.13}$$

of the trap in the tight axis, ν, is less than the spin healing length,

$$\xi_s = \frac{\hbar}{\sqrt{2M|g_s|n}}, \tag{2.14}$$

of the condensate. This means the variation in spin along this axis is essentially nullified and can be taken to be constant. The assumption is also made that the energy level gap of the tight harmonic trap, $\hbar\omega_\nu$, is significantly greater than any other energy being considered in the system so that all the bosons are thought to be in the ground harmonic state of the tight axis and that this state is the same for each of the hyperfine spin levels. For most of the experiments I have looked at [6–10] quasi-2D is the regime in which they work. I give the full reduction in appendix A but the general ideas needed are given here. For the reduction the wave-function components, ψ_m, are split into 2D, time dependent, wave-functions multiplied by the ground state of the tight axis harmonic oscillator. I take the tight axis to be the y-axis[3] which gives,

$$\psi_m(\mathbf{x}, t) = \psi_m^{xz}(x, z, t)\phi^y(y), \tag{2.15}$$

$$\phi^y(y) \approx \phi^{ho}(y) = \left(\frac{1}{\pi l_y^2}\right)^{\frac{1}{4}} \exp\left(-\frac{y^2}{2l_y^2}\right). \tag{2.16}$$

These equations are then substituted into the S1-GPE (2.9) for the wave-function. This is then all multiplied by ϕ^{y*} and integrated with respect to y (neglecting the zero point energy along y) to give,

$$\begin{aligned} i\hbar\frac{\partial\psi_m^{xz}}{\partial t} = &\left(-\frac{\hbar^2\nabla_{xz}^2}{2M} + V(x, z) - pm + qm^2\right)\psi_m^{xz} \\ &+ \frac{g_n}{\sqrt{2\pi}l_y}|\Psi^{xz}|^2\psi_m^{xz} + \frac{g_s}{\sqrt{2\pi}l_y}\sum_{m'=-1}^{m}\mathbf{F}^{xz}\cdot\mathbf{f}_{mm'}\psi_{m'}^{xz}, \quad (m = 1, 0, -1). \end{aligned} \tag{2.17}$$

Here,

$$|\Psi^{xz}|^2 = n(x, z), \tag{2.18}$$

[3]Taking the tight axis to be the y axis avoids any Zeeman shifting of the harmonic oscillator ground state. In most experiments I have read about this is also the case.

Is the total areal density. So the S1-GPE stays much the same in two dimensions except the interaction terms get scaled by a factor $1/\sqrt{2\pi}l_y$. This gives an obvious definition for the 2D interaction terms,

$$g_n^{2D} = \frac{g_n}{\sqrt{2\pi}l_y}, \quad g_s^{2D} = \frac{g_s}{\sqrt{2\pi}l_y}. \tag{2.19}$$

2.2.2 Non-Dimensionalisation of the S1-GPE

For computational purposes, dimensions can be time consuming and sometimes difficult to work with as using numbers with far different scales can introduce large computational errors. For this reason when simulating many systems it is easier to undimensionalise the equations of evolution first. In my simulations I consider a 2D system of bosons with uniform potential across the condensate ($V(x,z) = 0$). I then reduce the 2D S1-GPE by first introducing the dimensionless variables,

$$t = \tilde{t}t_0, \quad (x,z) = (\tilde{x},\tilde{z})x_0, \quad \rightarrow \quad \psi_m^{xz} = \frac{\tilde{\psi}_m^{xz}}{x_0}, \tag{2.20}$$

and subbing them in to 2.17, having removed the x, z superscripts,

$$\begin{aligned} \frac{i\hbar}{x_0 t_0}\frac{\partial\tilde{\psi}_m}{\partial\tilde{t}} &= \left(-\frac{\hbar^2\tilde{\nabla}^2}{2Mx_0^2} - pm + qm^2 \right)\frac{\tilde{\psi}_m}{x_0} \\ &+ \frac{g_n^{2D}}{x_0^2 x_0}\tilde{n}\tilde{\psi}_m + \frac{g_s^{2D}}{x_0^2 x_0}\sum_{m'=-1}^{m}\tilde{\mathbf{F}}\cdot\mathbf{f}_{mm'}\tilde{\psi}_{m'}, \quad (m = 1, 0, -1), \end{aligned} \tag{2.21}$$

recognising that ∇, n and $\mathbf{F}$ all have a dependence on ψ_m. Multiplying through by $x_0 t_0/\hbar$ gives,

$$\begin{aligned} i\frac{\partial\tilde{\psi}_m}{\partial\tilde{t}} &= \left(-\frac{t_0\hbar\tilde{\nabla}^2}{2Mx_0^2} - \frac{t_0}{\hbar}pm + \frac{t_0}{\hbar}qm^2 \right)\tilde{\psi}_m \\ &+ \frac{t_0 g_n^{2D}}{\hbar x_0^2}\tilde{n}\tilde{\psi}_m + \frac{t_0 g_s^{2D}}{\hbar x_0^2}\sum_{m'=-1}^{m}\tilde{\mathbf{F}}\cdot\mathbf{f}_{mm'}\tilde{\psi}_{m'}, \quad (m = 1, 0, -1). \end{aligned} \tag{2.22}$$

Setting,

$$t_0 = \frac{x_0^2 M}{\hbar}, \tag{2.23}$$

allows the defining of several dimensionless parameters,

$$\begin{aligned} q &= E_0\tilde{q}, \quad p = E_0\tilde{p}, \quad E_0 = \tfrac{\hbar^2}{x_0^2 M}, \\ g_n^{2D} &= G_0\tilde{g_n}, \quad g_s^{2D} = G_0\tilde{g_s}, \quad G_0 = \tfrac{\hbar^2}{M}. \end{aligned} \tag{2.24}$$

Subbing these back into equation 2.22 gives,

$$\begin{aligned} i\frac{\partial\tilde{\psi}_m}{\partial\tilde{t}} &= \Big(-\frac{\tilde{\nabla}^2}{2} - \tilde{p}m + \tilde{q}m^2 \Big)\tilde{\psi}_m \\ &+ \tilde{g}_n\tilde{n}\tilde{\psi}_m + \tilde{g}_s \sum_{m'=-1}^{m} \tilde{\mathbf{F}}\cdot\mathbf{f}_{mm'}\tilde{\psi}_{m'}, \quad (m = 1, 0, -1), \end{aligned} \tag{2.25}$$

which is the dimensionless, 2D S1-GPE. From now on I will refer to this equation as the S1-GPE and drop the tilde from the dimensionless parameters.

2.2.3 The Spin-1 Stochastic GPE

The S1-GPE works as a mean field description of a $T = 0$ condensate or as a multimode description of the condensate and its excitations (with added energy causing fluctuations). Without modification the S1-GPE can provide a description of a condensate system that is isolated and hence conserves particle number and energy, known as a micro canonical system, but attributing temperature and other entropy derivatives to this becomes challenging. To provide a simpler way of implementing a description of these terms it is useful to define the low energy single particle modes in the simulation as a classical region and considering all modes of higher energy to be part of an Incoherent region. For this classical field approximation we require the following from the two fields:

Classical (c) field region

This is the low energy region of appreciably occupied energy modes. It includes all modes with an energy less than a chosen cut-off energy. This region is evolved according to the S1-GPE, but now includes a projection term which excludes any modes that are considered to be outside the c-field region ($\epsilon_n > \epsilon_{cut}$).

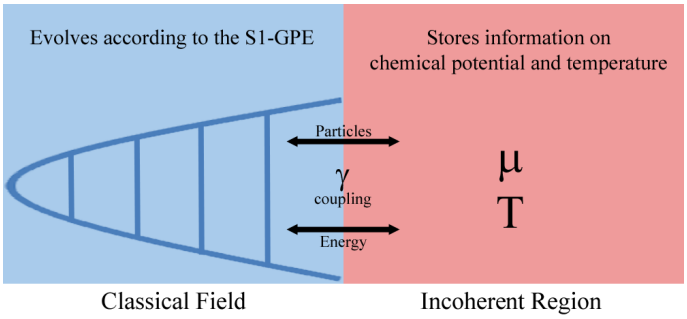

Figure 2.3: A model of the classical and Incoherent regions. The classical field stores information on the occupation of every energy mode within it and evolves according to the S1-GPE (2.9). The Incoherent region stores information on a thermal reservoir with a set chemical potential μ and temperature T. The two regions are coupled together by a coupling constant, γ, which allows the exchange of particles and energy.

Incoherent (I) region

This is the high energy region. Particles here are not simulated by the S1-GPE but are considered to be in equilibrium at some chosen temperature and density. The I-region couples with the c-field region through select interactions that introduce a temperature and chemical potential to the c-field dynamics, thus altering the S1-GPE.

The c-field region and I-region are demonstrated visually in Figure 2.3. The coupling between the regions can come through three different realistic mechanisms demonstrated in Figure 2.4. The code I am using only considers one interaction term, the two body I-region one, where particle interactions in the I-region lead to an exchange of particles and/or energy between the regions (Figure 2.4c). This simple growth is implemented into the system via additive noise terms in the evolution of the system. The exchange of particles and energy causes the I-region to act as a particle and energy reservoir to the c-field region meaning the c-field becomes grand canonical. The simple growth, stochastic (and nondimensional) S1-GPE (S1-SGPE) used in simulation is given below (equation 2.26). For a full description of the derivation

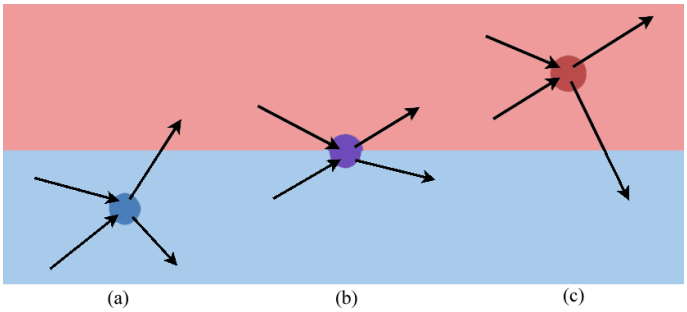

Figure 2.4: The allowed physical interactions between the c-field region (blue) and the I-region (red) are shown. They are (a) between two c-field atoms causing one to leave the c-field, (b) between a c-field atom and an I-region atom in which number in which the c-field number is conserved (scattering) and (c) between two I-region atoms causing one to drop into the c-field (growth). Figure adapted from [18].

and details of this algorithm see [19].

$$\begin{aligned} d\psi_m = -(\gamma + i)\Bigg[\Bigg(-\frac{\nabla^2}{2} - pm + qm^2 - \mu\Bigg)\psi_m \\ + g_n n\psi_m + g_s \sum_{m'=-1}^{m} \mathbf{F}^{xz} \cdot \mathbf{f}_{mm'}\Bigg] dt + i\sqrt{\gamma T} \cdot \frac{\mathbb{C}(\text{noise})\sqrt{dt}}{\sqrt{dV}}, \end{aligned} \tag{2.26}$$

where the μ and T are the chemical potential and temperature respectively and γ is a term that controls the coupling of the c-field and I regions and triggers the growth of the system towards an equilibrium described by μ and T. It then dampens any shift from equilibrium once reached. A high γ will cause the system to reach equilibrium quickly, whereas a low γ can be used to examine growth effects. For $\gamma = 0$ this reduces to the S1-GPE and energy, number and magnetisation in the c-field becomes conserved. The noise introduced is complex in nature and scaled according to the purely computational terms, simulation step size, dt, and volume of the grid spacing, dV.

Chapter 3

Important Background Literature

The single most important text I have read this year is a Physics Report review by Yuki Kawaguchi and Masahito Ueda, titled "Spinor Bose-Einstein condensates" [15]. Published in 2012 Kawaguchi and Ueda collected all the current knowledge of the spinor Bose systems into one article. It is an authoritative reference on spin-1 condensates (as well as for spin-2 and spin-3) and has been of great help to me during my research.

3.1 The Berkeley ^{87}Rb Experiments

From 2005 the group at the University of California, Berkeley, did a series of experiments on spin-1 ^{87}Rb condensates that began with demonstrating an in-situ technique of imaging the condensate and subsequent applications of this technique to study the dynamics of this system. All their experiments were conducted in quasi-2D and they imaged along this tight axis, which they generally called the y-axis (for this dissertation I adopt this convention also). Typically they achieved condensates with a population of two to four million bosons with peak densities of around $2 \times 10^{14}\text{cm}^{-3}$. Much of my introduction to this area of physics was done through reading this series of papers to understand the basic cold atom physics and the properties of spinor condensates. My research led on from this as I attempted to develop the code to a point where it could be used to simulate their results on finite temperature domain formation. Here I briefly describe three of the experiments, the first

two describing the onset of the idea and techniques for trapping and exploring the mechanics of the spin-1 system and the third talking about one of their experiments that involved reaching equilibrium from an uncondensed initial state, the results of which I attempt to simulate in my work.

3.1.1 J.M. Higbie et al. "Direct Nondestructive Imaging of Magnetization in a Spin-1 Bose-Einstein Gas" [6]

This was their first experiment and its main goal was to demonstrate their technique for imaging the magnetisation of the spin-1 ^{87}Rb without destroying the condensate. They prepared their sample to have all the population in the $m = -1$ hyperfine spin level with a magnetic field along the z-axis of the system defining the quantisation axis. The systems spin vector was then tipped using a $\pi/2$ rf pulse, to be transverse to the magnetic field. This caused the spin to undergo Larmor precession around the z-axis at about 38 kHz. Using dispersive imaging they measured the y-component of magnetisation along a thin strip of the condensate as the spin precessed around the magnetic field. An example of this imaging, sampled at 20 kHz, is shown in Figure 3.1. The Larmor precession amplitude decayed with time indicating a decay in the number of particles having a transverse magnetisation. To find whether this effect on the condensate was purely due to loss of particles or a mix of loss of particles and particles rotating back to a longitudinal polarization the group compared a tip and hold method with a hold and tip method

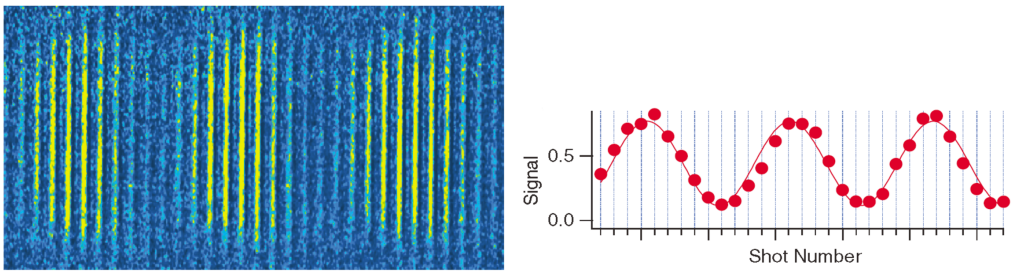

Figure 3.1: The y-axis magnetisation is imaged in 31 consecutive shots. The image shows the Larmor precession as a periodic modulation of the intensity of the response. 38 kHz Larmor precession is aliased with the 20 kHz causing an oscillation of the peak signal strength. From ref. [6].

for both a condensate and a thermal cloud. The tip and hold method involved tipping with the rf pulse at $t = 0$ and allowing evolution of the system to occur before measuring the Larmor precession amplitude, thus allowing for decay via number loss and spin rotation, whereas the hold and tip method let the system evolve before tipping and measuring, thus measuring the precession amplitude for only loss of number. Their results are shown in Figure 3.2. The Larmor precession amplitude decay rate of the condensate was very close between the hold and tip and tip and hold methods suggesting that in the condensate the only loss of particles with spin in the transverse plane was to particles leaving the system. In the thermal cloud the decay rate was an order of magnitude faster in the tip and hold method than the hold and tip method suggesting the opposite to the condensate, that there are many particles in the thermal cloud returning to a longitudinal spin orientation. This shows that the condensate is key in the process of keeping the particles in the transversely magnetised state. The group concludes that the imaging technique they use opens up many opportunities to investigate unexplored properties of spinor condensates.

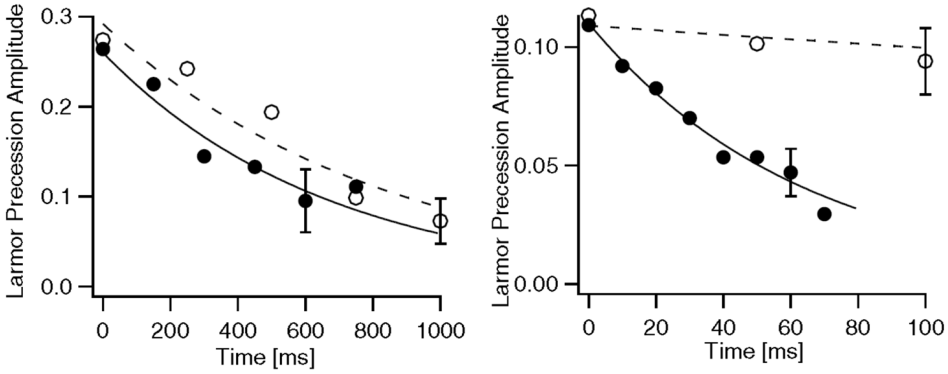

Figure 3.2: The decay of the Larmor precession amplitude is shown for (a) a BEC and (b) a thermal cloud. Tip and hold (filled circles) and hold and tip (open circles) are compared. The decay of Larmor precession in a BEC is almost the same for the tip and hold and hold and tip methods, whereas in the thermal cloud the tip and hold decays by almost a factor of 10 faster. From ref. [6].

3.1.2 L.E. Sadler et al. "Spontaneous symmetry breaking in a quenched ferromagnetic spinor Bose-Einstein condensate" [7]

This paper was published in Nature. In it they described the phase transition between the polar phase and the BA phase and demonstrated the broken rotational symmetry in the BA phase. Their system is prepared, using a 2 G magnetic field aligned in the transverse plane, as a condensate deep in the polar phase ($q \gg 2|g_s|n$), where almost all of the bosons occupy the $m = 0$ hyperfine spin level. At $t = 0$ they lower the quadratic Zeeman energy, by orienting the magnetic field in the z-axis and shifting it linearly over 5 ms to 50 mG, to quench the system deep into the BA phase ($q \ll 2|g_s|n$, see fig. 2.3). The linear Zeeman shift is neglected due to spin conservation. The system's magnetisation in the y-axis was imaged as in [6]. The spatial distribution of magnetisation was detected by finding the amplitude, A, and relative phase, ϕ, of the Larmor precession across the condensate ($A(\mathbf{x})\exp(i\phi(\mathbf{x})) = in(\mathbf{x})(F_x(\mathbf{x}) + iF_y(\mathbf{x}))$. At the time of the quench there is no magnetisation in the system, longitudinal or transverse. Sometime after the quench (> 50ms) they found transverse magnetisation that varied in direction across the condensate had spontaneously developed, thus indicating the breaking of SO(2) rotational symmetry around the z-axis. The effect this had on the system was to form domains of like transverse spin that grew to fill the condensate, with different domains separated by unmagnetised domain walls or continuous variation of spin from one domain to another, as shown in Figure 3.3. They then gave a reason for the spontaneous magnetisation of the condensate and formation of domains, the reason being that the $m = 0$ initial state in the z-axis is a superposition of $m_{transverse} = \pm 1$ states. Because of the ferromagnetic property of ^{87}Rb ($g_s < 0$) any $m = \pm 1$ states are immiscible, meaning a small fluctuation in the transverse magnetisation will cause oppositely magnetised bosons to separate, influence other bosons and hence neighbouring domains grow that have oppositely oriented transverse magnetisation. Domain walls can then be described as overlaps between the neighbouring regions, hence they have no net magnetisation. The rest of the paper is devoted to showing features of the magnetised condensate. They showed that in the BA phase any longitudinal magnetisation is small and does not grow after the quench, that the spatial correlation of the transverse magnetisation grows from uncorrelated to alternating positive and negative

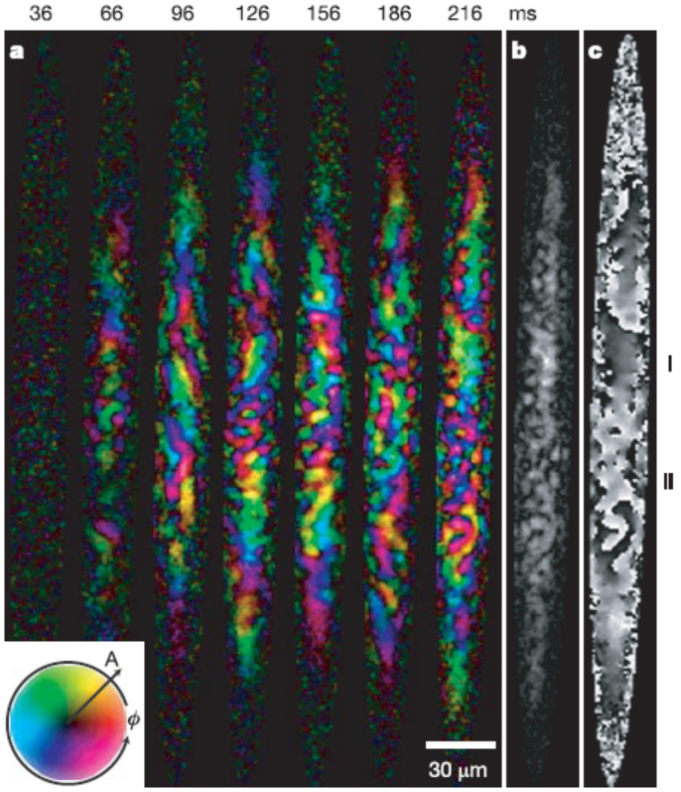

Figure 3.3: (a) The transverse magnetisation density of the condensate at variable times is shown with orientation of magnetisation given by the colour and strength by the brightness as shown by the colour wheel on the left. The magnetisation density (b) and orientation (c) are shown separately for the $t = 206\,ms$ case. Gradual change of the orientation can be seen in region I whereas small domains at region II are separated by domain walls with zero magnetisation. From ref. [7].

correlations over short distances, supporting the observation that neighbouring domains have opposite magnetisation. Lastly they showed examples of spin vortices, points with unmagnetised cores about which the direction of transverse magnetisation rotates by 2π. They finish by describing that domain walls are not stable and may decay through the formation of spin vortex-antivortex pairs, but that some domain walls survive the lifetime of the condensate. Because of this they suggested that in future experiments they would take a closer look at the dynamical evolution of the domain walls and vortices and suggested that slowing down the quench could uncover other dynamics of the phase transition.

3.1.3 J. Guzman et al. "Long-time-scale dynamics of spin textures in a degenerate F=1 ^{87}Rb spinor Bose gas" [10]

This paper was published in 2011. In this work they looked at the effect of cooling atoms to the desired parameters from different spinor populations in an initial uncondensed thermal cloud. The thermal cloud was prepared above the critical temperature for condensation to have a fraction of the population in each of the $m = \pm 1$ states, $f_{\pm 1}$, equal to 1/3, 1/4 or 0, so that the net longitudinal magnetization was 0. It was then cooled to well below the critical temperature so that a condensate could form and grow. They did this for a range of quadratic Zeeman, $-45\text{Hz} < q/h < 45\text{Hz}$ ($2|g_s|n \approx h \times 8\text{Hz}$). They studied the length of time the system took to evolve towards the expected equilibrium states from the original population differences. What they found was that inside a range $-5\text{Hz} < q/h < 5\text{Hz}$ the system evolved towards the expected state in approximately two seconds. Even up to $|q| < h \times 10\text{Hz}$ the populations were seen to be heading towards the expected population distribution. Outside this region however the original spin populations are maintained throughout the lifetime of the condensate. Their results are demonstrated in Figure 3.4. They suggest that the reason for the strong mixing dynamics at low $|q|$ occurs because spin-mixing is primarily happening in the condensed part of the system and has little influence on the thermal part of the system. Following this they present results showing the spatial distribution of magnetisation in both the longitudinal axis and transverse plane for low values of q. Their images are shown in Figure 3.5. The phase change from the BA phase to the Ferromag-

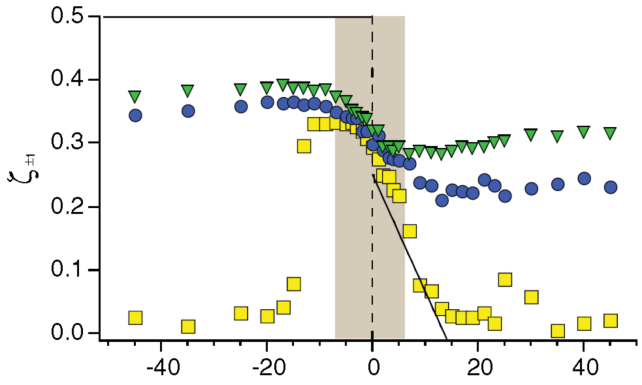

Figure 3.4: The population fraction in each of the $m = \pm 1$ hyperfine spin levels at 2 s is shown for original fractions 1/3 (green triangles), 1/4 (blue circles) and 0 (yellow squares). In the shaded region the populations have evolved towards a common steady state in agreement with mean field predictions (black line). Outside that region the initial population fractions persist for the lifetime of the condensate. From ref. [10].

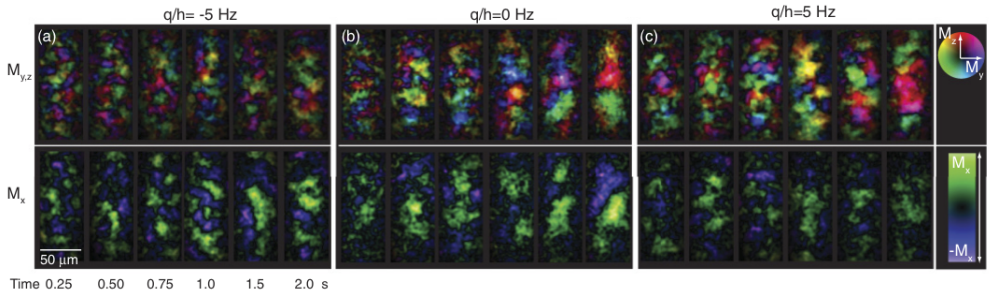

Figure 3.5: Transverse (top) and longitudinal (bottom) magnetisation is shown after variable evolution time up to 2 s for the quadratic shifts shown above the figures (note: the group changed their magnetic field axis to the x-axis for this experiment. This is now the longitudinal axis). For late times there is a spin space anisotropy; for positive q the transverse magnetisation is brighter whereas for negative q the longitudinal magnetisation appears brighter. From ref. [10].

netic phases is demonstrated by the change from a large amount of transverse magnetisation for $q > 0$ compared to a large amount of longitudinal magnetisation for $q < 0$. At the boundary, $q = 0$ there is a mix of both transverse and longitudinal magnetisation as one would expect at the phase transition. Lastly they note that spin domains form and grow from the spontaneous magnetisation to sizes reaching $40\,\mu$m in 2 seconds. They suggest that the domain length plateaus here although their data (Figure 3.6) does not appear to be entirely conclusive. To conclude they stated the four trends they had observed: a redistribution of hyperfine spin level populations from initial fractions, the development of spontaneous magnetisation, the development of spin space anisotropy and the coarsening of spin domains. All of these trends occur for small $|q|$ and on a similar 1-2s timescale. They note that for larger q equilibrium is not reached within the timescale of the experiment but note that the spin-mixing time, $\tau = h/(2|g_s|n)$ is significantly smaller than the seconds long equilibrium times. The interpretation and understanding of these results is hampered by a lack of theory for the thermal dynamics.

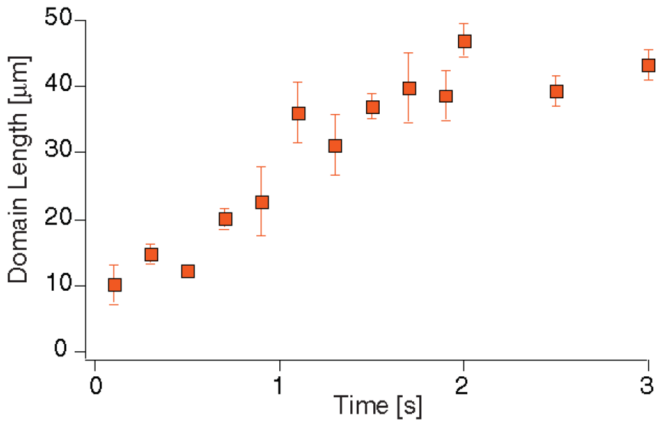

Figure 3.6: Evolution of domain length within the system for a quadratic shift of 0 Hz and original fraction $f_{\pm 1} = 1/3$. The domain length grows smoothly as a function of the evolution time with final values of around $40\,\mu$m being observed within 2 s. From ref. [10].

Chapter 4

Validating and Exploring the Code

For simulating the system of spin-1 bosons I have inherited a new Stochastic GPE code developed over summer by a project student. The code is for general use in a variety of cold bosonic systems, not primarily spinor cases. It had not yet been well tested and required extensive testing and validation before it could be properly used. The code is expected to behave in certain ways that reflect the true evolution of spin-1 bosons at low temperatures. This means it has to adhere to certain conservation laws such as number and spin conservation in an isolated system. It must also behave in particular ways in terms of the ground state solutions of the S1-GPE expected at low temperatures. This chapter highlights the development of the tools and testing of the code I went through to verify everything was working correctly. All equations in this chapter are for dimensionless units.

4.1 Validation

4.1.1 Conservation Laws

In an isolated system one would expect there to be no loss or gain in number of particles or energy. As mentioned in section 2.1.2 the spin interactions between two particles conserve total spin. This gives us another conservation law where the difference between the population in the $m = 1$ to $m = -1$ hyperfine spin levels (i.e. total z magnetisation) must remain a constant in an

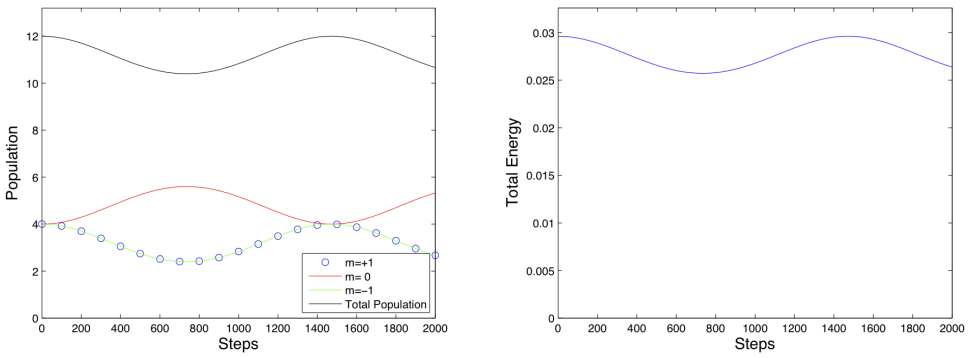

(a) (b)

Figure 4.1: The original code had violated number conservation (a) caused by the loss (or gain) of one $m = 0$ boson for the gain (or loss) of one each of $m = \pm 1$ bosons. As can be seen (b) this causes a change in energy in the system also. [Each step has $dt = 0.05$, $g_s(g_n) = -0.5(0.5)$ and $p(q) = 0.05(0)$]

isolated system. Isolating my system by setting γ to zero, and thus preventing any interaction with the incoherent region, I can test the conservation laws and confirm that they are working. Figure 4.1 shows an example of this, with energy calculated as the energy per particle given in equation 2.11 added up across the whole system, plus the total kinetic energy in the system calculated by summing the kinetic energy over the occupation of the momentum space grid for each hyperfine spin level, $E_k = dV_k \sum_{m,\mathbf{k}} |\phi_{mk}(\mathbf{k})|^2 \mathbf{k}^2/2$, where dV_k is the areal grid spacing. As can be seen there was a problem with the conservation of number (Figure 4.1a) and energy (Figure 4.1b). It appeared as though for each $m = \pm 1$ pair of bosons being created there was only one $m = 0$ boson being lost, causing the number to increase or decrease depending on during the spin oscillations. This was fixed by identifying a missing factor of 2 in an interaction term in the code. Past this fix we observe that in the isolated system number and energy conservation laws are obeyed (Figure 4.2).

4.1.2 Grand Canonical Ensemble

As discussed in section 2.2.3, the simple growth S1-SGPE ($\gamma \neq 0$) is subject to a grand canonical description. To test this we consider an ideal (non-interacting, $g_s = g_n = 0$) case, where the occupation of the single particle

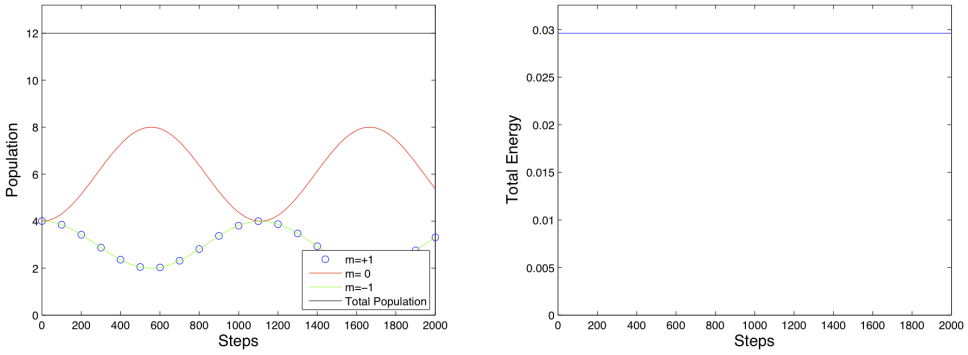

(a) (b)

Figure 4.2: The figures show conservation of number and energy. The z magnetisation is also a constant, shown here as the difference between the $m = \pm 1$ populations. [Same parameters as Figure 4.1]

energy modes (i.e. the momentum modes on the computational grid) can be predicted [20]. In grand canonical equilibrium the mean occupation of a mode of energy, ϵ, is given by the Bose-Einstein distribution,

$$N_{BE}(\epsilon) = \frac{1}{\exp\left(\frac{\epsilon-\mu}{T}\right) - 1}, \tag{4.1}$$

where μ and T are the chemical potential and temperature respectively. However this assumes integer occupied microstates whereas in the classical approximation we are not restricted to this and the distribution is given by the classical limit known as equipartition,

$$N_{eq}(\epsilon) = \frac{T}{\epsilon - \mu}. \tag{4.2}$$

In my simulations the possible energy states are given by the momentum modes on the simulation grid. Because of the periodic boundary conditions these modes can take on particular momentum values that match with wavelengths across the classical field. As a first test we consider no Zeeman shifts, $p = q = 0$, so that all spin states have the same energy modes and we can neglect spin in our analysis. We would expect the momentum modes to have an average occupancy given by 4.2 with energy, $\epsilon_k = \mathbf{k}^2/2$. To test this we ran a stochastic S1-GPE simulation where we evolve a system from random

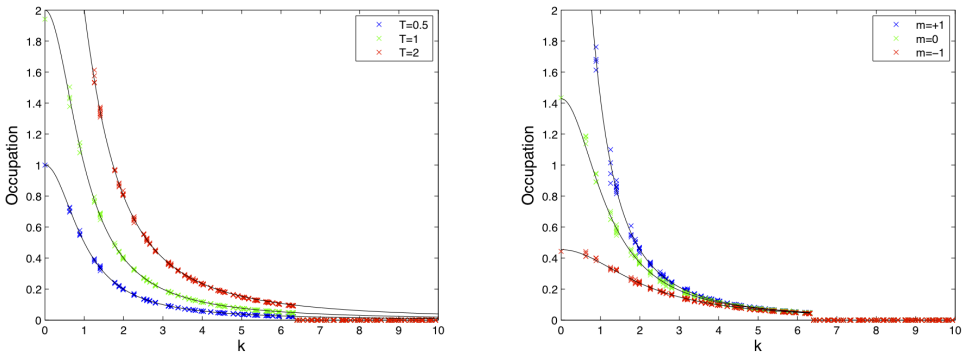

(a) (b)

Figure 4.3: Ideal tests of the stochastic S1-GPE are shown. (a) p=q=0, the hyperfine levels are degenerate and the system behaves as if it is a scalar Bose gas. The momentum mode occupations are shown for $T = 0.5, 1$ and 2 and all achieve good fit with the predictions (black lines). (b) $2q = p = 1$, the momentum mode occupations are satisfied at $T = 1$ for each spin level. Results were calculated using $\mu = -0.7$ and $\gamma = 1$. Note the c-field limit at $k > 6.2$ where occupation drops to zero.

initial conditions for long enough to equilibiate, i.e. the c-field atom number stops growing predictably and varies around some mean value. We note that identifying equilibrium is difficult as the system keeps fluctuating. After equilibrium we evolve for the system for 10^4 time steps and find the average occupancy of the momentum modes. The momentum mode amplitudes (ϕ) of the field can be found by finding the Fourier transform of the spatial representation of the wave-function. Plotting the kinetic energy, ϵ_k, of each of the momentum modes against the time averaged occupation of the mode,

$$N_k = \overline{|\phi(\mathbf{k})|^2} dV_k, \tag{4.3}$$

where,

$$dV_k = \left(\frac{2\pi}{L}\right)^2, \tag{4.4}$$

is the momentum cell volume. I could then compare the predictions with the results shown in Figure 4.3a. The single particle energies are shifted by the Zeeman effects, hence the energy of a momentum mode depends on the kinetic energy of the mode and the hyperfine spin level it acts in, $\epsilon_{k,m} =$

$\epsilon_k - pm + qm^2$. This means each of the hyperfine spin levels are expected to have a different occupation distribution,

$$N_{eq}(\epsilon, m) = \frac{T}{\epsilon_k - pm + qm^2 - \mu}. \tag{4.5}$$

Comparing the different spin predictions again gets good agreement between the mean occupation and the predicted occupation, with an example shown in Figure 4.3b.

4.1.3 Ground State Phases

The phase diagrams in Figure 2.2 predict the ground state spinor at zero temperature under different conditions. To validate the interaction effects of the code we can investigate whether the known ground states are obtained for $T = 0$. To do this we solved the S1-GPE with $T = 0$, but μ and γ non-zero. This case is known as the damped S1-GPE and should evolve to a ground state that satisfies,

$$\mu\psi_m = \left(-\frac{\nabla^2}{2} - pm + qm^2\right)\psi_m + g_n n\psi_m + g_s \sum_{m'=-1}^{m} \mathbf{F}\cdot\mathbf{f}_{mm'}\psi_{m'}, \quad (m = 1, 0, -1), \tag{4.6}$$

with the hyperfine population fractions as given by the ground state spinor. In the following I took $\gamma = 10$, $\mu = 10$, $g_n = 0.05$ (which gives $n \approx \mu/g_n = 200$) and evolved an initially even share of population among the hyperfine spin levels to $t = 30$. This was done for various combinations of p, q and g_s where different ground states are expected (see Figure 2.2 for the phase diagram)

Ferromagnetic and Polar Phases

These phases exist for both positive and negative values of g_s and hence can be tested for either value. Each phase predicts a ground state with all of the bosons in a single hyperfine spin level. During evolution I would expect the fractional population of only the appropriate level to go up to 1 and the population of the others to go to zero. The results of such a simulation are shown in Figure 4.4.

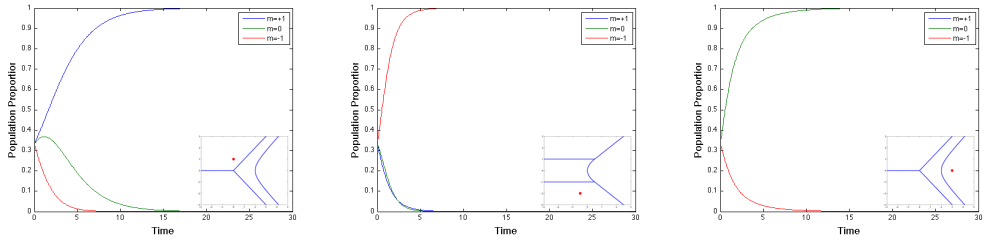

(a) Ferromagnetic +1 (b) Ferromagnetic −1 (c) Polar

Figure 4.4: The Ferromagnetic and Polar ground states are satisfied by the damped S1-GPE. The appropriate hyperfine spin population quickly gains all the population. For a,b,c, $|g_s| = 1 \times 10^{-4}$ with the sign being $-+-$ respectively, and $q\,(p) = 0\,(|g_s|n)$, $-|g_s|n/2\,(-2|g_s|n)$ and $3|g_s|n\,(0)$ respectively.

Anti-Ferromagnetic Phase

In the AF ground state there is predicted to be occupation of both of the $m = \pm 1$ hyperfine spin levels with the fraction of the total population in each given as follows [15]:

$$|\zeta_{\pm 1}|^2 = \frac{1}{2}\left(1 \pm \frac{p}{g_s n}\right). \tag{4.7}$$

This is seen to be obtained in Figure 4.5a.

Broken-Axis Phase

The BA phase has a ground state population that occupies all three hyperfine spin levels. The predicted population fractions are given in equations (4.8) and (4.9) [15].

$$|\zeta_{\pm 1}|^2 = \left(\frac{q \pm p}{2q}\right)^2 \left(\frac{-p^2 + q^2 + 2g_s nq}{2g_s nq}\right) \tag{4.8}$$

$$|\zeta_0|^2 = \frac{(q^2 - p^2)\,(-p^2 - q^2 + 2g_s nq)}{4g_s nq^3} \tag{4.9}$$

The results of simulations in this phase match the predictions as shown in Figure 4.5b.

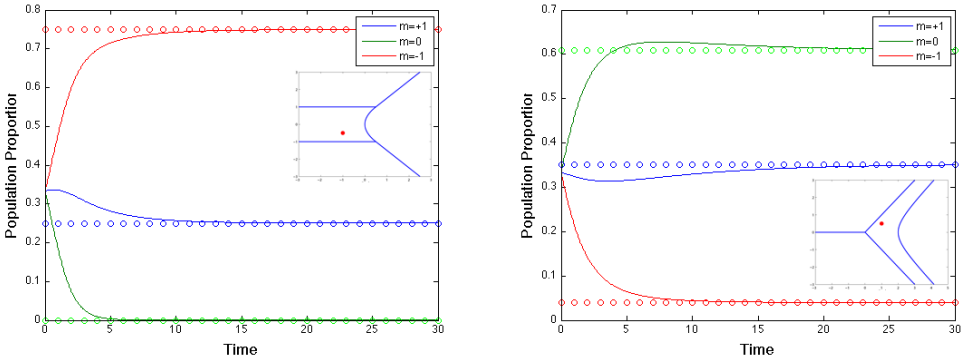

(a) Anti-Ferromagnetic ($g_s > 0$) (b) Broken-Axis ($g_s < 0$)

Figure 4.5: The AF and BA ground states are satisfied by the damped S1-GPE. The fractional populations (lines) evolve towards their predicted amounts (circles) for each of the phases. It takes longer than the singly occupied phases, with the BA phase in particular taking almost the whole time to reach the expected population spread. For the AF run (a) $g_s = 1 \times 10^{-4}$ and $q(p) = -|g_s|n(-|g_s|n/2)$ and for the BA run (b) $g_s = -1 \times 10^{-4}$ and $q(p) = |g_s|n(|g_s|n/2)$

4.2 Multiple Chemical Potentials

Having performed a range of code validations I went on to consider controlling the spin populations. The motivation was that in the experiment by Guzman et al. [10], the initial spin populations of the above critical temperature states were varied and we would like to have this control. I decided to consider the effects of giving each hyperfine spin level its own chemical potential. What this involves is replacing μ in the stochastic S1-GPE (equation 2.26) with μ_m, where $(\mu_{+1}, \mu_0, \mu_{-1})^T$ is a vector of the three different chemical potentials. I found that any shift in the chemical potential affected the spin level populations that would evolve, but more importantly shifting it by amounts significantly more than the Zeeman differences essentially removed the effects of the Zeeman energies and the chemical potential controlled how the population was divided among the spin levels. A comparison between a single μ example and a multiple μ example is shown in Figure 4.6, where the multiple μ are shifted by an amount equal to the linear Zeeman, up for $m = \pm 1$ and down for $m = 0$. While this seems like it's not a good thing there are some advantages to this. Systems can be prepared in thermal clouds to have particular (non-equilibrium) fractional populations in each of

the spin levels, the experiment by J. Guzman et al. [10] described in section 3.1.3 is one such example. While I can prepare my c-field region to have particular spin level populations, having only one chemical potential means we cannot produce equilibrium initial conditions similar to those initial (non-equilibrium) states prepared in experiments. Making use of multiple chemical potentials may be a way around this.

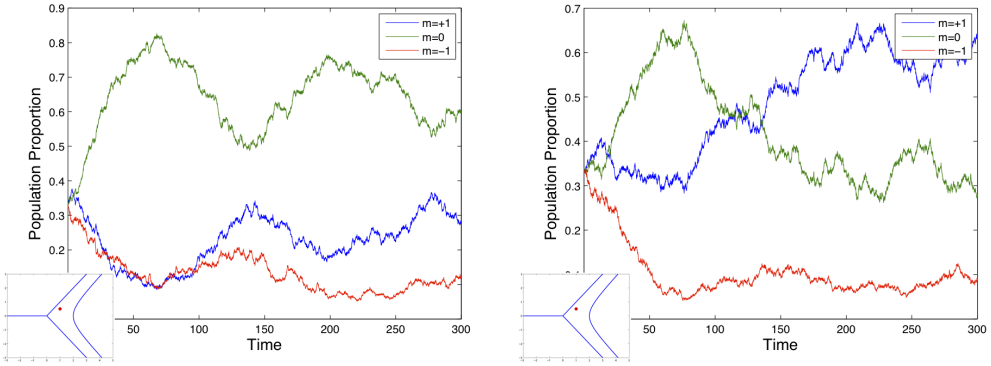

(a) Single Chemical Potential $\mu = 10$ (b) Multiple Chemical Potentials $[\mu_{+1}, \mu_0, \mu_{-1}] = [10.01, 9.99, 10.01]$

Figure 4.6: The figures show typical examples of evolution of the hyperfine spin populations as a fraction of the total population for $T = 10$, $\gamma = 0.25$ and g_n, g_s, p and q as they were in the BA phase test earlier (section 4.1.3). The shift in chemical potential is exactly equal to the linear Zeeman energy, shifting up for $m = \pm 1$ and down for $m = 0$. As can be seen the $m = 0$ population fraction goes way down whereas the $m = +1$ fraction goes way up.

Chapter 5

Comparison to Guzman et al.

Here we aim to apply the S1-SGPE as a simplified finite temperature qualitative model of the experiments of Guzman et al. [10], discussed in chapter 3.

5.1 Initial State

To simulate the cooling quench we need to find initial conditions for the S1-SGPE that are similar to that of the experimental conditions. In particular the experiment began at high temperatures far above the critical temperature with the fractional population in the $m = \pm 1$ states given by,

$$|\zeta_{+1}|^2 = \frac{N_{+1}}{N} = |\zeta_{-1}|^2 = \frac{N_{-1}}{N}, \tag{5.1}$$

so there is no magnetisation present.

5.1.1 Parameters

They use ^{87}Rb atoms in the experiment for which the values of g_n and g_s are known [15]. Their tight axis trap frequency was $\omega_y = 2\pi \times 480\,\text{Hz}$, which gives a characteristic harmonic oscillator length of $l_y = 0.492\,\mu\text{m}$. Table 5.1 gives the experimental values considered and the corresponding values in computational units from chapter 2, with $x_0 = 1\,\mu\text{m}$; e.g. measurements in the experiment are made on timescales in the range $t = 0.2 \to 4\,\text{s}$, in our computational units this corresponds to $t = 146 \to 2920$.

Table 5.1: Typical experimental values are given for the parameters in the Guzman experiment along with the dimensionless units chosen for my simulations and the corresponding computational values. The experimental g_n and g_s are the 3D interaction terms calculated from the scattering lengths for ^{87}Rb given in Table 2.1 using equations 2.5 and 2.6. The computational g_n and g_s are for a 2D system.

Parameter	Experimental Range or Value	Dimensionless Unit	Computational Range or Value
Length	$1 \rightarrow 120\,\mu$m	$1\,\mu$m	$1 \rightarrow 120$
Time	$0.2 \rightarrow 4\,$s	$1.37 \times 10^{-3}\,$s	$146 \rightarrow 2920$
Quadratic Zeeman	$0 \rightarrow 8\,$Hz$\times$h	$116\,$Hz$\times$h	$0 \rightarrow 0.0687$
g_n	$5.17 \times 10^{-51}\,$Jm^3	$9.52 \times 10^{-50}\,$Jm^3	0.0543
g_s	$-2.48 \times 10^{-53}\,$Jm^3	$9.52 \times 10^{-50}\,$Jm^3	-2.60×10^{-4}
Temperature	$50 \rightarrow 350\,$nK	$5.59\,$nK	$8.95 \rightarrow 62.7$

Discrepancies

I obtained the mean areal density I would need for the computational system by looking at the quadratic Zeeman shift quoted for the phase transition for the polar to the BA phase, $q_t = 8\,\text{Hz} \rightarrow 0.0687$ in dimensionless units. I then used the relationship that is satisfied at the phase transition, $2|g_s|n = q_t$, to find the areal density I would need to match the experiment. This gave $n = 132$. I then found an appropriate chemical potential that produced the right density ($\mu = 7.1 \approx g_n n$). The critical temperature T_c for condensation of the Berkeley experiments is quoted as being around 350 nK [9] which equates to $\sim$63 in dimensionless units. I ran simulations to find the critical temperature for my system. These simulations were run until they reached equilibrium with $\gamma = 0.25$. From there they were allowed to run for $t = 200$ and the mean population and mean condensate population during this time were found. This was done for $T = 0 \rightarrow T = 80$. We are considering a uniform potential approximation to the experiment, therefore we expect the critical temperature will be different to the 63 given above. What I expected to see was the condensate population to show a trend towards zero near this value. My results are shown in Figure 5.1. There is a discrepancy. Although I expected a little bit of difference between the expected T_c and the T_c I found, this difference seems very large. Going back to the paper I looked at

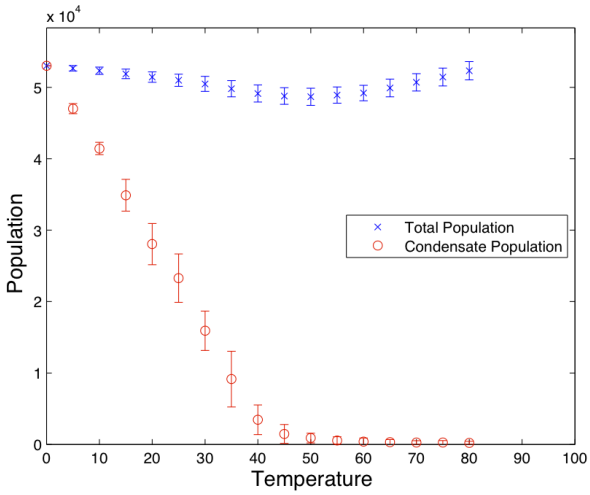

Figure 5.1: The mean total population and condensate population is shown for a variety of temperatures. Error bars are calculated as twice the standard error of the data in each direction. The expected trend was for the condensate population to drop to zero around $T = 60$, this appears to go to zero around $T = 40$.

the density they had quoted as their average density in the y-direction after 2 s, $\langle n_y \rangle = 1.85 \times 10^{14}\,\mathrm{cm}^{-3}$, which is the value they use in the relationship $q_t = 2|g_s|\langle n_y \rangle = h \times 8\,\mathrm{Hz}$. Working backwards I find $g_s = -1.433 \times 10^{-53}\,\mathrm{Jm}^3$, almost a factor of two less than what I got from the scattering lengths. This can occur because there is some uncertainty in the s-wave scattering lengths. Therefore, g_s, which is given by the difference between the scattering lengths has a large uncertainty. Because of this uncertainty I have taken a dimensionless value for g_s ($= 1.51 \times 10^{-4}$) that matches with the experimental value found in this paragraph and a chemical potential that gives a critical temperature around 63, $\mu = 10$. The new temperature trend is shown in Figure 5.2.

5.1.2 The Incoherent Region

The last section has been considering c-field population only. To understand our entire system it is necessary to account for all of the atoms above the c-field region in the I-region. Because the I-region atoms have a high kinetic energy and a low phase space density, interaction effects are less important and the I-region population can be approximated by the ideal Bose-Einstein

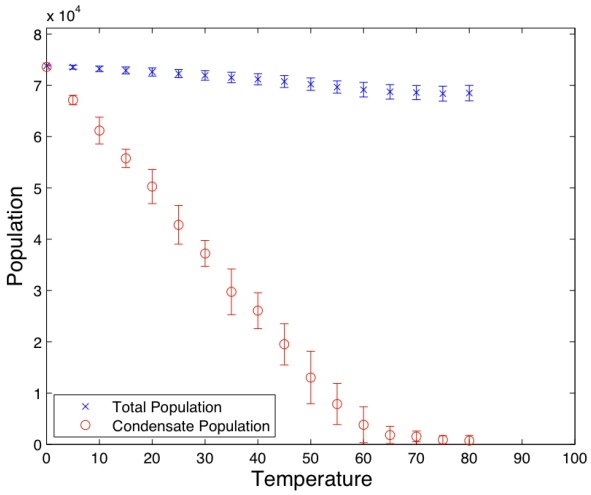

Figure 5.2: The condensate population now has a trend towards zero around 60 as expected.

distribution (equation 4.1).

Finding the Incoherent Region Population

To find the I-region population I need to know the allowed states in the I-region and the expected occupation of them. To do this I find a density of states and calculate the expected occupation of these states with the Bose-Einstein distribution. For a full derivation of the density of states see appendix C. My system is a 2D square of width w with periodic boundary conditions. This means there are only certain allowed wavelengths in each axis,

$$\lambda_\nu = 2w, w, \frac{2w}{3}, ..., \frac{2w}{n_\lambda}, \quad \nu = x, z. \tag{5.2}$$

The total number of states with an energy less than ϵ_k is,

$$G(\epsilon_k) \approx \frac{w^2 \epsilon_k}{2\pi}, \tag{5.3}$$

which approximates the discrete kinetic energy levels as continuous. This can then be differentiated with respect to ϵ_k to give the density of states in our computational units,

$$g(\epsilon_k) = \frac{w^2}{2\pi}. \tag{5.4}$$

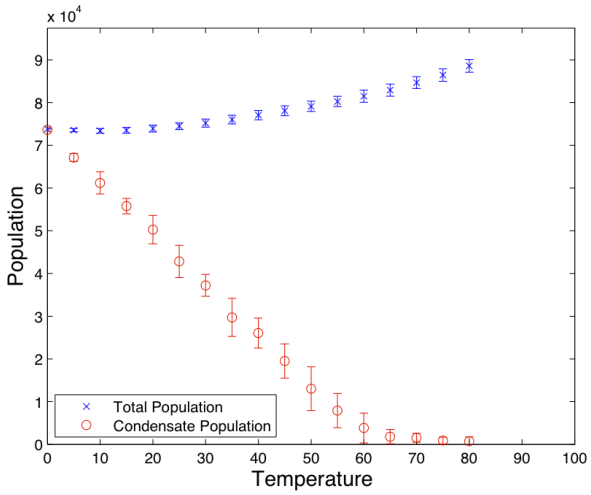

Figure 5.3: Including the population assumed to be in the Incoherent region causes the mean population to rise with temperature.

Notably in 2D it is constant. Combined with the distribution of particles an expected population for a range of energies can be found by multiplying the two together and integrating with respect to ϵ_k. The total number of incoherent atoms for a spin level is given thus,

$$\begin{aligned} N_{Im} &= \int_{\epsilon_{cut}}^{\infty} g(\epsilon_k) N_{BE}(\epsilon_k - pm + qm^2)\,\mathrm{d}\epsilon_k \\ &= \frac{w^2}{2\pi}\left(\epsilon_{cut} - pm + qm^2 - T\log\left[\exp\left(\frac{\epsilon_k - pm + qm^2 - \mu}{T}\right) - 1\right]\right). \end{aligned} \tag{5.5}$$

Figure 5.3 shows the same data as in Figure 5.2 with the added I-region population. The total population goes up with temperature, this is expected as the chemical potential is the same for every temperature. To produce a result for constant total number would require iterated adjustment of the chemical potential for each temperature. Keeping the total number constant with temperature is not important for us, we are more concerned with the condensate and spin level population fractions. I am now in a position to examine at what temperature the condensate fraction shows a trend towards zero and find a critical temperature for my system. Figure 5.4 shows a linear

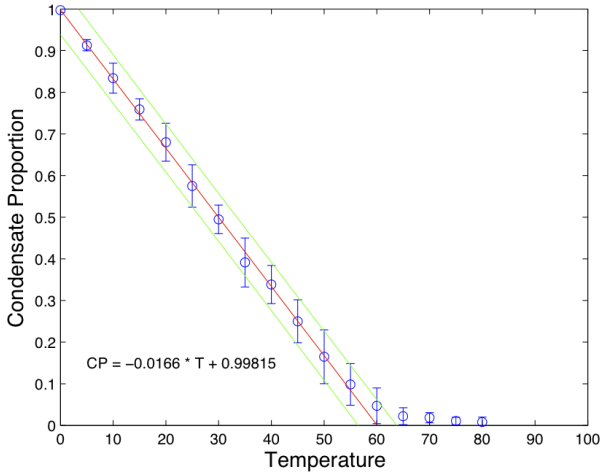

Figure 5.4: This figure shows the mean fraction of the population that occupies the condensate (blue circles) and a linear fit (C_F) to all but the last five temperatures (red line, green lines indicate twice the standard error), hence excluding points that have error bars that reach or very nearly reach zero. The fit goes to zero at 60 suggesting the critical temperature for condensation in this computational system is $T_c = 60$.

trend towards zero condensate at $T = 60$[1].

Comparison to expected hyperfine populations

As a simple prediction I proposed that in the condensate the population fractions would match with the predicted ground state fractions given in equations 4.7, 4.8 and 4.9, whereas the thermal cloud, neglecting Zeeman effects, would exhibit no spin ordering and be evenly distributed across the three spin levels, giving the following relationship for a spin level fractional population,

$$|\zeta_m|^2 = C_F|\zeta_m^G|^2 + (1 - C_F)/3, \tag{5.6}$$

where C_F is the condensate fraction and G indicates the ground state. Figure 5.5 compares the systems behaviour from the same data used in Figure 5.3 up to and above T_c. We observe reasonable agreement between the simulated

[1]The condensate population does not go completely to zero as the S1-SGPE assumes $T < T_c$ at all times.

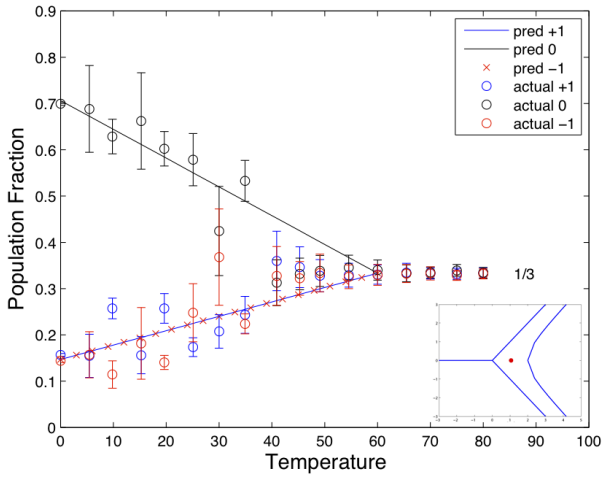

Figure 5.5: The hyperfine spin fractions are given for individual runs at each temperature (circles) as well as the simple prediction given in the text.

populations and our simple model.

5.1.3 Finding the Initial Wave-Function

Initially the Berkeley group start with a sample of ^{87}Rb that is at a temperature $\gg T_c$. They put this population into a state where there is no longitudinal magnetisation and a particular fraction of the population in each hyperfine spin level ($|\zeta_{\pm 1}|^2 = 1/3, 1/4, 0$). They then cool it through the critical temperature down to a final temperature of 50 nK. We take $t = 0$ to be at the end of the cooling. Due to time constraints I only considered one initial case, $|\zeta_{\pm 1}|^2 = 1/3$. To simulate the cooling quench I created a thermal wave-function and used it as the initial wave-function for simulations at $t = 0$. This essentially considers the cooling to occur instantaneously. To make the thermal wave-function I assume that equilibrium is reached quickly in the thermal cloud meaning the cooling effects are not significant until just above the critical temperature. This means that I only need to find an initial wave-function at a temperature a small amount above the critical temperature. The chemical potential goes to zero in this regime and I take the Zeeman terms to be zero also so the hyperfine spin levels are degenerate and should, on average, be equally occupied. With these parameters I allow the

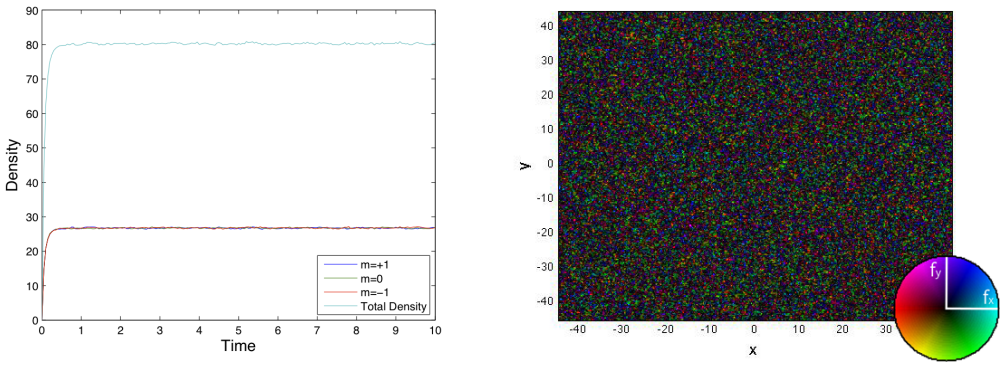

(a) (b)

Figure 5.6: Figure (a) shows the total (light blue) and individual hyperfine spin level populations from finding the initial wave-function. There is an 1/3, 1/3, 1/3 share of population between the levels as was wanted. Figure (b) shows the distribution of magnetisation within the system. It is highly unmagnetised and randomly oriented right across the system.

system to run until it is in equilibrium and use this as the initial thermal wave-function. Having established the initial conditions for my simulation I am now in a position to find the correct growth rate of the system.

5.2 Growth Rates

Guzman et al. quenched their system down to a final temperature, $T = 50\,\mathrm{nK}$ for a range of quadratic Zeeman. Figure 3.6 shows the growth of the domain length in the experimental system for zero quadratic Zeeman. To get similar results I want to adjust gamma so that the system grows similar domains on the same sort of time scales. In principle the value of γ could be determined by a detailed understanding of the I-region. In practice this is not well understood for a spinor system in 2D. For this reason we take γ as a parameter to be determined by ensuring the quench behaviour, i.e. domain growth, occurs over a similar timescale in the simulations as it does in the experiment. To measure the domain size the group measured the spatial correlation of the x, y and z-axis magnetisation and then measured the area, A, of the central positive region of the sum of these three correlations. They

then defined the typical domain length of the system as,

$$l = \sqrt{\frac{4A}{\pi}}, \tag{5.7}$$

the diameter of a circle of area A. They claimed that the domains grew to around $40\,\mu$m in about 2 s and then stayed around this value for the rest of the experimental time. By adjusting γ I can change the growth of the system to match their domain sizes. What I am looking for is a particular gamma for the parameters in my system that causes the domains to grow to the expected size in the equivalent of 2 s and then stay this size for the rest of the simulation.

5.2.1 Measuring the Domain Size

I measure the domain length up to a maximum of $50\,\mu$m in my system by finding the spatial correlation, C, of the spin density for each of the axes,

$$C_\nu(dx, dz) = \sum f_\nu(x, z) \times f_\nu(x + dx, z + dz), \quad (\nu = x, y, z), \tag{5.8}$$

adding them up for each shift and then counting the number of shift points within 25 of the centre point that has positive (greater than noise) correlation. A fully ordered gas will produce a domain length of 50 counting this way. This correlation function and domain size procedure was chosen to match with what they used in the Guzman experiment as closely as possible. An example of how the domain length is found is given in Figure 5.7.

Initially I had no idea what value for γ was going to be suitable other than it was going to be small, so I tried a range of γ from 10^{-2} to 10^{-5}. I found $\gamma \approx 10^{-2}$ was most suitable as the domain growth appeared to occur on a similar timescale to experiments, see Figure 3.6. Exploring γ values around 10^{-2} yielded the results in Figure 5.8 There appeared to be a problem with the domain length increasing to lengths beyond my maximum measurement of 50 no matter what γ was and not reaching a plateau as observed in experiment. Looking at the xy spin of the system (Figure 5.9) it appears to be because the system may not have been big enough to handle domain sizes of 40 without them consuming the system due to the periodic boundary conditions causing them to interfere with themselves. I had been using a system that had a width of twice the expected domain length. Figure 5.10 gives the results

for a system of width 120, three times the expected domain size. Again the domain length appeared to not plateau (Figure 5.11 shows a system nearly filled by one domain). There appeared to be a problem with the way I was working with the code. I had assumed it was the temperature that would cause the domains to not get any larger as I assumed the noise would put a ceiling on how large the domains could get. But a potential issue is that when the system has cooled, i.e. significantly condensed with domains, that the approximation of the I-region as a reservoir may break down.

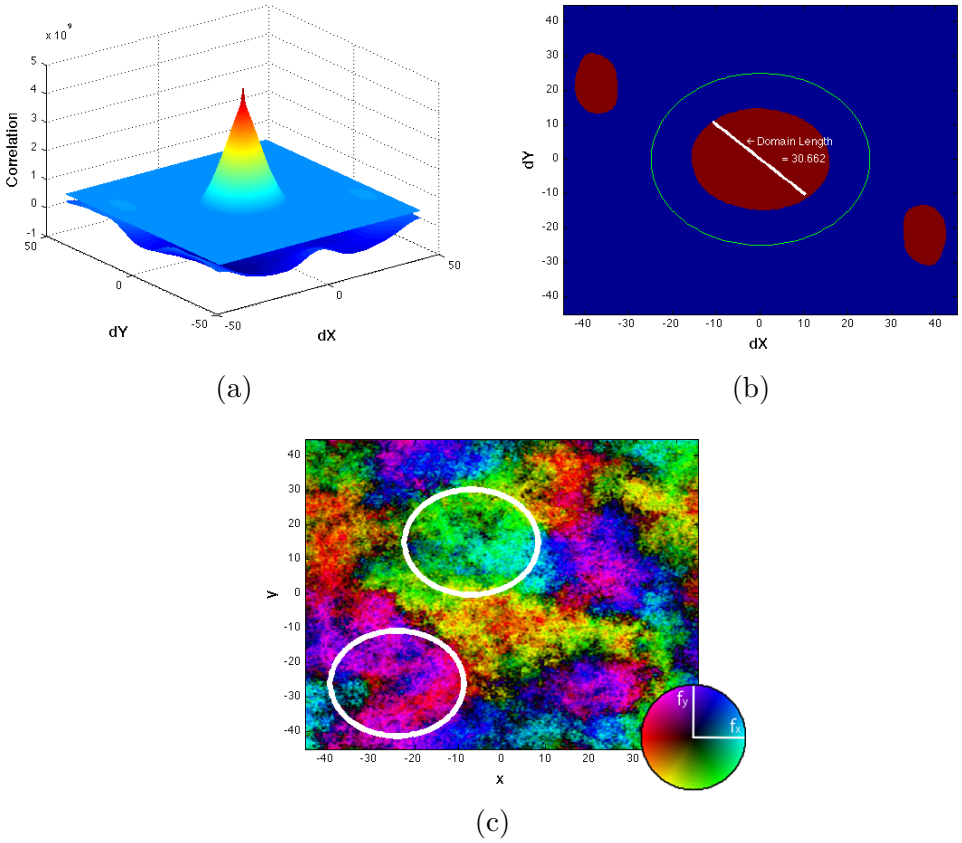

(a) (b)

(c)

Figure 5.7: An example showing how the domain length of the system is measured. The spatial correlation function is calculated with shifts measured from the centre (a). Every point with a correlation more than 10% is then found (red sections in (b)). The area of these correlations that does not have a shift of more than 25 from the centre (green circle in (b)) is then found. The domain length is considered to be the diameter of a circle that has this area. Figure (c) shows an example of what the domain size looks like on the transverse plane.

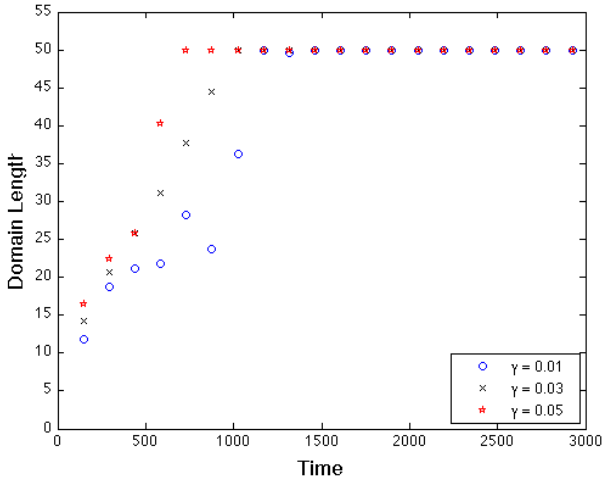

Figure 5.8: The domain length versus time for various values of γ, other simulation parameters are mentioned in the text. Note that $t = 1000$ corresponds to 1.37 s. (c.f. experimental result in Figure 3.6)

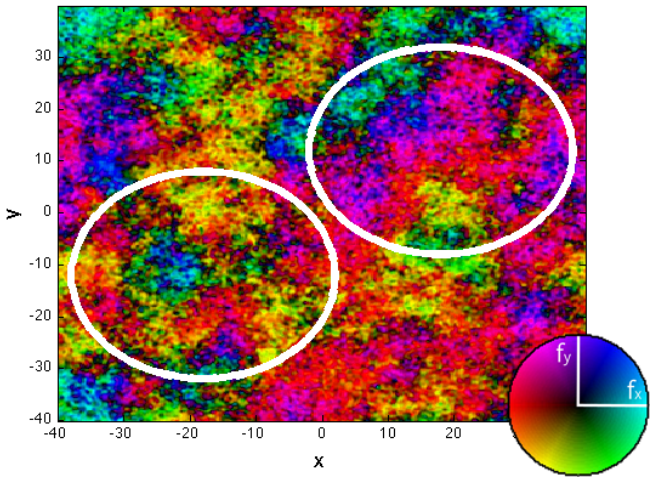

Figure 5.9: The system may be too small to handle the domain size. Two domain circles are shown at the expected size and they fill just about the whole system. This spatial spin distribution is

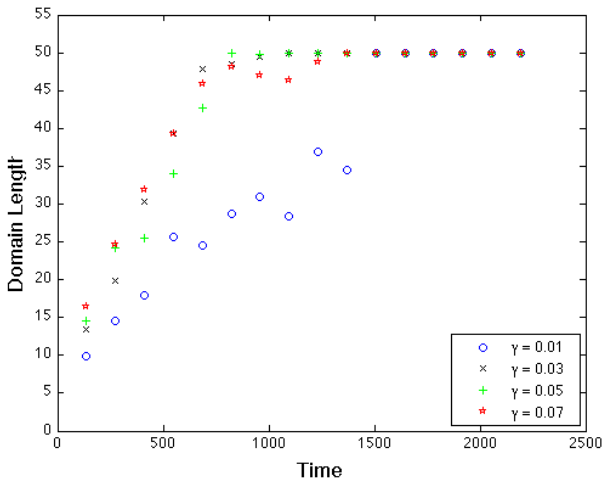

Figure 5.10: Increasing the size of the field did not help. The domain length still goes past 40 to saturation at 50.

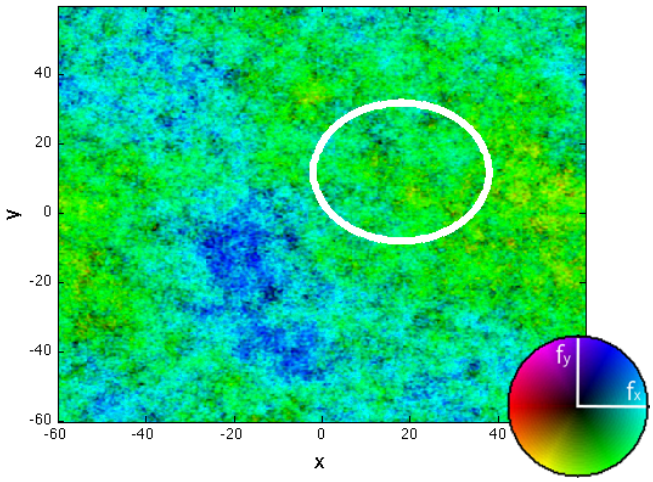

Figure 5.11: Shows a single domain to have almost consumed the condensate. This is for the last recorded time in the $\gamma = 0.07$ run shown in Figure 5.10. A circle of diameter 40 is superimposed to show the expected range of the domains.

5.2.2 Introducing a Cut-Off Time

In the last section I allowed a thermal wave-function to evolve under the influence of a reservoir and found that a single domain would completely fill the system, contrary to the experimental example where it is expected to plateau around 40. We proposed that once the system has cooled that considering an I-region may become invalid. The only reason I really want the gamma there is to introduce the correct population to the system with the correct energy for the temperature being simulated. After that it is no longer needed and can be cut off, i.e. setting $\gamma = 0$ at some time into the simulation to mimic the I-region becoming depleted. The system then evolves according to the non-linear dynamics in the c-region alone.

Because I know that a γ of 0.01 is nearly appropriate I use it and try cutting it off at four values, equivalent to 200 ms, 500 ms, 1 s and 1.5 s, before the domains are fully formed. The resulting domain lengths are shown in Figure 5.12. The domains length appears to be limited. At the very least the growth time of the domains have been slowed by the cut off. Two of the cut-off times reach the domain length of 40 being sought after and one (cut-off at $t = 1100$) stays around that length for the remainder of the simulation. Figure 5.14 shows the change in the amount of particles in the c-field region for each of the cut-offs. Each of the cut-off simulations reaches the equilibrium population before being cutoff, after which the population loss can be put down to computational loss.

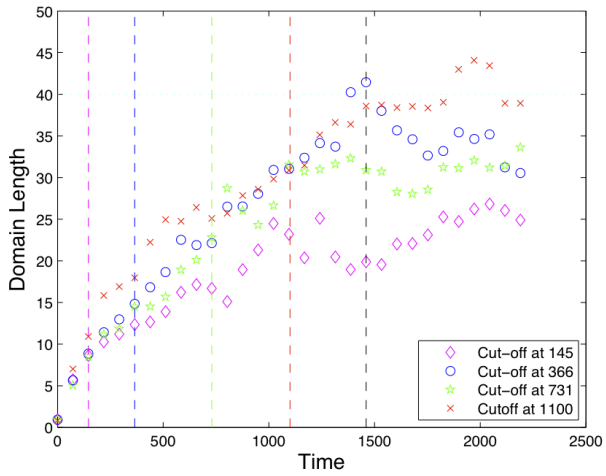

Figure 5.12: Evolution of the system from an initial thermal state is shown for an initial $\gamma = 0.01$ getting cut off at various times given in the legend. The vertical coloured lines indicate the time each sample was cut off and the black vertical line indicates 2 s, the time the system is expected to reach domain lengths of 40. Domain growth has decreased considerably from before suggesting the cut-off is preventing the system from becoming fully magnetised. This simulation was run with $p = q = 0$.

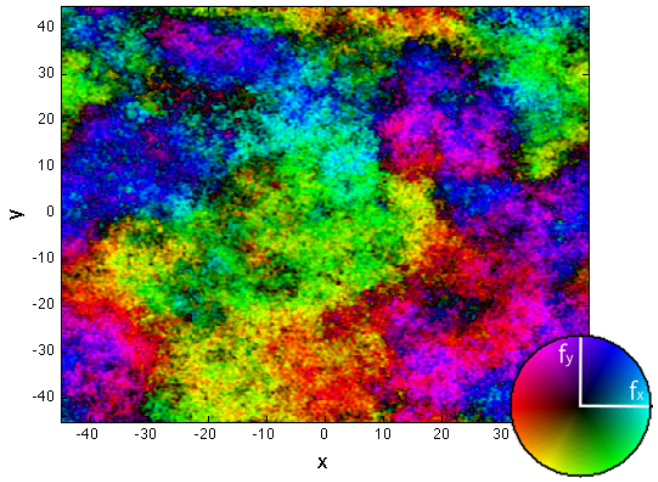

Figure 5.13: To give an idea of what a system with the expected domain length looks like the distribution of transverse spin at 2 s is shown for $\gamma = 0.01$, having been cut- off at 1.5 s (red x in Figure 5.12 that intersects with the black line)

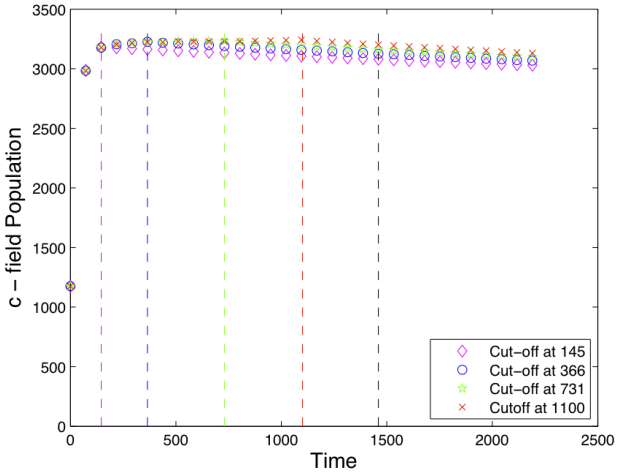

Figure 5.14: The c-field population of the simulations. As shown γ is kept on for long enough to allow the population to rise to the equilibrium value. Any loss after γ is set to zero is down to computational loss. The vertical lines indicate the same as they did for Figure 5.12

Chapter 6

Conclusion and Future Work

The major achievements of this research are as follows:

The validation of the S1-SGPE

The code I received at the start was relatively new and had not been tested extensively or validated for the spin-1 case. We were able to take the code and run it through a series of tests to ensure satisfied required criteria. This was done for an isolated system, which showed the code had a significant error, and after being fixed it then satisfied conservation laws for total number, energy and magnetisation; an ideal system, where energy mode occupations without interactions were shown to obey grand canonical theory as expected; and the damped S1-GPE, which showed that the system at zero temperature did evolve towards the expected spinor ground states.

Development of a method to simulate a temperature quench

By making a few assumptions we were able to develop a method for simulating an experiment that quenched a system down from a high temperature to below T_c. We assumed the gas at high temperature would thermalize quickly meaning we only consider the dynamics from when the system passed through the critical temperature. Allowing a simulation to run just above the critical temperature, with no Zeeman or chemical potential, until it reached equilibrium then gave us a thermal spatial wave-function with a third of the population in each of the hyperfine spin levels, just as in the experiment. We then assumed the quench from to $T = 50\,\mathrm{nK}$, was instantaneous by

putting the thermal wave-function as an initial condition and evolving with the stochastic S1-GPE with the final temperature and chemical potential.

Qualitative agreement with experiments using a new technique

We showed that the code could qualitatively demonstrate some of the features of the experiment, most notably the growth of the domains. We explored the range of γ values to ensure the domain growth was quantitatively similar to experiments. The use of a cut-off time for γ limited the influence the reservoir could have on the c-field region and this translated into restricting the growth of the domains.

Our results suggest the stochastic S1-GPE is a feasible approach for studying finite temperature quench dynamics in this system, in fact it is currently the only easily controllable method for these regimes. Future work will be to explore more experimental observations, e.g. the effect of different initial population fractions prior to a quench; testing effects of the energy cut-off on simulations, thus increasing the extent of the c-field; exploring the quadratic Zeeman dependence of the quench, as was done by Guzman et al. (Figure 3.4); and implementing scattering interaction terms into the stochastic S1-GPE theory, terms that simulate interaction (b) in Figure 2.4.

Bibliography

[1] S. N. Bose, "Plancks gesetz und lichtquantenhypothese," *Zeitschrift für Physik*, vol. 26, no. 178, 1924.

[2] E. A., "Quantentheorie des einatomigen idealen gases," *Sitzungsberichte der Preussischen Akademie der Wissenschaften*, vol. 1, no. 3, 1925.

[3] M. H. Anderson, J. R. Ensher, M. R. Matthews, C. E. Wieman, and C. E. A., "Observation of bose-einstein condensation in a dilute atomic vapor," *Science Reports*, vol. 269, pp. 198–201, July 1995.

[4] D. Stamper-Kurn, M. Andrews, A. Chikkatur, S. Inouye, H.-J. Miesner, J. Stenger, and W. Ketterle, "Optical confinement of a bose-einstein condensate," *Physical Review Letters*, vol. 80, pp. 2027–2030, November 1998.

[5] M.-S. Chang, C. Hamley, M. Barrett, J. Sauer, K. Fortier, W. Zhang, L. You, and M. Chapman, "Observationofspinordynamicsinopticallytrapped 87rb bose–einstein condensates," *Physical Review Letters*, vol. 92, no. 140403, 1992.

[6] J. M. Higbie, L. E. Sadler, S. Inouye, A. Chikkatur, S. R. Leslie, K. L. Moore, V. Savalli, and D. M. Stamper-Kurn, "Direct nondestructive imaging of magnetization in a spin-1 bose-einstein gas," *Physical Review Letters*, vol. 95, July 2005.

[7] L. E. Sadler, J. M. Higbie, S. R. Leslie, M. Vengalattore, and D. M. Stamper-Kurn, "Spontaneous symmetry breaking in a quenched ferromagnetic spinor bose-einstein condensate," *Nature*, vol. 443, pp. 312–5, Sep 2006.

[8] S. R. Leslie, J. Guzman, M. Vengalattore, J. D. Sau, M. L. Cohen, and D. M. Stamper-Kurn, "Amplification of fluctuations in a spinor bose-einstein condensate," *Physical Review A*, vol. 79, April 2009.

[9] M. Vengalattore, J. Guzman, S. R. Leslie, F. Serwane, and D. M. Stamper-Kurn, "Periodic spin textures in a degenerate f = 1 87rb spinor bose gas," *Physical Review A*, vol. 81, May 2010.

[10] J. Guzman, G.-B. Jo, A. N. Wenz, K. W. Murch, C. K. Thomas, and D. Stamper-Kurn, "Long-time-scale dynamics of spin textures in a degenerate f = 1 87rb spinor bose gas," *Physical Review A*, vol. 84, December 2011.

[11] T.-L. Ho, "Spinor bose condensates in optical traps," *Physical Review Letters*, vol. 81, no. 4, pp. 742–5, 1998.

[12] C. Law, H. Pu, and N. Bigelow, "Quantum spins mixing in spinor bose-einstein condensates," *Physical Review Letters*, vol. 81, pp. 5257–5261, December 1998.

[13] J. Stenger, S. Inouye, D. M. Stamper-Kurn, H.-J. Miesner, A. Chikkatur, and W. Ketterle, "Spin domains in ground-state bose-einstein condensates," *Nature*, vol. 396, pp. 345–8, September 1998.

[14] H. Saito and M. Ueda, "Spontaneous magnetization and structure formation in a spin-1 ferromagnetic bose-einstein condensate," *Physical Review A*, vol. 72, August 2005.

[15] Y. Kawaguchi and M. Ueda, "Spinor bose-einstein condensates," *Physics Reports*, vol. 520, pp. 253–381, 2012.

[16] D. M. Stamper-Kurn and M. Ueda, "Spinor bose gases: Symmetries, magnetism, and quantum dynamics," *Reviews of Modern Physics*, vol. 85, pp. 1191–1244, July 2013.

[17] M. Vengalattore, S. R. Leslie, J. Guzman, and D. M. Stamper-Kurn, "Spontaneously modulated spin textures in a dipolar spinor bose-einstein condensate," *Physical Review Letters*, vol. 100, May 2008.

[18] E. Linscott, "Non-zero temperature theory for ultra-cold dipolar bose gases," Master's thesis, University of Otago, 2013.

[19] P. Blakie, A. Bradley, M. Davis, R. Ballagh, and C. Gardiner, "Dynamics and statistical mechanics of ultra-cold bose gases using c-field techniques," *Advances in Physics*, vol. 57, pp. 363–455, September-October 2008.

[20] D. V. Schroeder, *An Introduction to Thermal Physics*. Addison Wesley Longman, 1999.

Appendices

Appendix A

Reduction to Two-Dimensions

–

We begin with the wave -function, ψ_m, in three dimensional form and the S1-GPE as in equation 2.9,

$$\begin{aligned} i\hbar\frac{\partial\psi(\mathbf{x},t)}{\partial t} &= \bigg(-\frac{\hbar^2\nabla^2}{2M} + V(\mathbf{x}) - pm + qm^2 \bigg)\psi_m \\ &+ g_n n\psi_m + g_s \sum_{m'=-1}^{m} \mathbf{F}\cdot\mathbf{f}_{mm'}\psi_{m'}, \quad (m = 1, 0, -1). \end{aligned} \tag{A.1}$$

We then assume that all the particles are in the ground state of the y-axis harmonic trap and that this does not change with time. The wave-function can then be decomposed into an xz time dependent part and a time independent y part as follows,

$$\psi_m(\mathbf{x},t) = \psi_m^{xz}(x,z,t)\phi^y(y) \tag{A.2}$$

where,

$$\phi^y(y) \approx \phi^{ho}(y) = \bigg(\frac{1}{\pi l_y^2}\bigg)^{\frac{1}{4}} \exp\bigg(-\frac{y^2}{2l_y^2}\bigg), \tag{A.3}$$

$$\int_{-\infty}^{\infty} |\phi(y)|^2 \,\mathrm{d}y = 1. \tag{A.4}$$

For the system I consider the potential is taken to be uniform in the xz-plane hence the trapping potential energy becomes,

$$V(\mathbf{x}) = \frac{M\omega_y^2 y^2}{2} \tag{A.5}$$

Plugging A.2 and A.5 into A.1, multiplying $\phi^y(y)^*$ and integrating with respect to y, remembering that n and $\mathbf{F}$ depend on ψ, gives,

$$\begin{aligned} i\hbar\frac{\partial\psi_m^{xz}}{\partial t} = &-\frac{\hbar^2(\nabla^{xz})^2}{2M}\psi_m^{xz} - pm\psi_m^{xz} + qm^2\psi_m^{xz} \\ &+ \frac{1}{2}\psi_m^{xz}\left(-\frac{\hbar^2}{M}\int_{-\infty}^{\infty}\phi^{y*}\frac{\partial^2}{\partial y^2}\phi^y\,\mathrm{d}y + M\omega_y^2\int_{-\infty}^{\infty}y^2|\phi^y|^2\,\mathrm{d}y\right) \\ &+ g_n(n^{xz})^2\psi_m^{xz}\int_{-\infty}^{\infty}|\phi^y|^4\,\mathrm{d}y + g_s\sum_{m'=-1}^{m}\mathbf{F}^{xz}\cdot\mathbf{f}_{mm'}\psi_{m'}^{xz}\int_{-\infty}^{\infty}|\phi^y|^4\,\mathrm{d}y, \quad (m=1,0,-1). \end{aligned} \tag{A.6}$$

Because we know ϕ^y we can evaluate the integrals.

$$\frac{\partial^2}{\partial y^2}\phi^y(y) = \frac{y^2}{l_y^4}\phi^y - \frac{1}{l_y^2}\phi^y, \tag{A.7}$$

$$\begin{aligned} &\left(-\frac{\hbar^2}{M}\int_{-\infty}^{\infty}\phi^{y*}\left(\frac{y^2}{l_y^4}\phi^y - \frac{1}{l_y^2}\phi^y\right)\mathrm{d}y + M\omega_y^2\int_{-\infty}^{\infty}y^2|\phi^y|^2\,\mathrm{d}y\right) \\ &\quad = \left(-\frac{\hbar^2}{Ml_y^4}\int_{-\infty}^{\infty}y^2|\phi^y|^2\,\mathrm{d}y + \frac{\hbar^2}{Ml_y^2} + M\omega_y^2\int_{-\infty}^{\infty}y^2|\phi^y|^2\,\mathrm{d}y\right). \end{aligned} \tag{A.8}$$

Subbing back in expression 2.15 for l_y the two remaining integrals cancel and we are left with a constant $\hbar\omega_y/2$. This is the zero point energy along the y-axis and hence can be ignored and removed from the equation. The final integral,

$$\int_{-\infty}^{\infty}|\phi^y|^4\,\mathrm{d}y = \frac{1}{\sqrt{2\pi}l_y}, \tag{A.9}$$

gives us this two dimensional form of the GPE,

$$\begin{aligned} i\hbar\frac{\partial\psi_m^{xz}}{\partial t} = &-\frac{\hbar^2(\nabla^{xz})^2}{2M}\psi_m^{xz} - pm\psi_m^{xz} + qm^2\psi_m^{xz} \\ &+ \frac{g_n}{\sqrt{2\pi}l_y}(n^{xz})^2\psi_m^{xz} + \frac{g_s}{\sqrt{2\pi}l_y}\sum_{m'=-1}^{m}\mathbf{F}^{xz}\cdot\mathbf{f}_{mm'}\psi_{m'}^{xz}, \quad (m=1,0,-1). \end{aligned} \tag{A.10}$$

Two dimensional interaction terms can then also be defined as such,

$$g_n^{2D} = \frac{g_n}{\sqrt{2\pi}l_y}, \quad g_s^{2D} = \frac{g_s}{\sqrt{2\pi}l_y}, \tag{A.11}$$

leaving us with the two dimensional uniform S1-GPE,

$$\begin{aligned} i\hbar\frac{\partial\psi_m^{xz}}{\partial t} &= \left(-\frac{\hbar^2(\nabla^{xz})^2}{2M} - pm + qm^2 \right)\psi_m^{xz} \\ &+ g_n^{2D}(n^{xz})^2\psi_m^{xz} + g_s^{2D}\sum_{m'=-1}^{m}\mathbf{F}^{xz}\cdot\mathbf{f}_{mm'}\psi_{m'}^{xz}, \quad (m=1,0,-1). \end{aligned} \tag{A.12}$$

Appendix B

Dipolar Effects in a Spin-1 System

B.1 M. Vengalattore et al. "Spontaneously Modulated Spin Textures in a Dipolar Spinor Bose-Einstein Condensate" [17]

For this paper the Berkeley group showed that the dipolar interaction of the ^{87}Rb atoms can have an influence on the evolution and equilibrium states of the spin-1 system. The dipolar interaction may be parametrised by a length, $a_d \approx 0.4|a_2 - a_0|$, that is comparable to the difference in s-wave scattering lengths, which implies the dipolar interaction could have a significant impact comparable to the spin interaction. To test this they prepared their system in a similar way to [6], preparing all the bosons in the $m = -1$ hyperfine spin level and then tipping them into the transverse plane. However they make one change now by comparing the evolution of a system where all bosons have been tipped to have the same spin to one where the spin varies in helical fashion along the z-axis of the condensate. Figure B.1 shows the results. The uniform spin remains essentially homogeneous for the lifetime of the condensate, whereas the helical structure breaks up into small domains similar to that of the quench in the Nature paper [7]. They also note that during the breakup of the helical structure the kinetic energy per particle increased dramatically to levels far higher than the initial energy stored in the helix due to accounted for energies (thermal, spin and potential). They

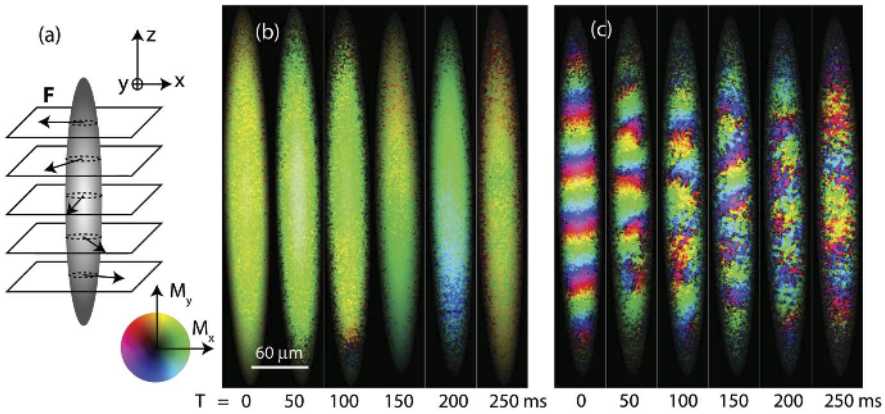

Figure B.1: Spontaneous breakup of helical structure in a ^{87}Rb spin-1 Bose-Einstein Condensate. A system of all bosons tipped in the same direction causing a uniform spin texture is shown in (b) whereas a system prepared in helical fashion is shown in (c). (a) demonstrates the rotation of the spin orientation along the z-axis of the condensate. Trasverse magnetisation is measured for various times. The uniform texture remains uniform for long evolution times whereas the helical structure dissolves into short range order over short times ∼200 ms

state that this apparent deficit can be accounted for by including dipole-dipole interactions. To test if the dipole-dipole interactions were causing the breakup of the helical structure they re-ran the helical tests but this time introduced rapid spin rotations during the evolution. These rotations were intended to cause the anisotropic dipole interactions to average out to zero while leaving the isotropic contact interactions unaffected. Figure B.2 shows some of the effects of attempting to nullify the dipole interactions. They did not achieve perfect removal of the breakup of the system but noted that it was significantly hampered suggesting that the long range dipolar forces were being diminished. This suggests that the dipolar forces do have a significant effect on the system and thus cannot always be ignored when studying spinor systems.

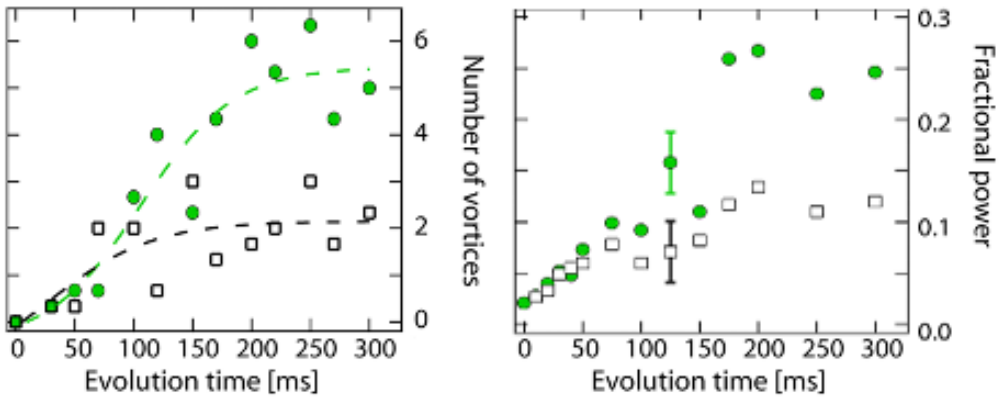

Figure B.2: The evolution of the helical structure with (white squares) and without (green circles) rapid spin rotation. The number of vortices counted in the system at various evolution times is lowered significantly and the fractional power of short range modulations is lowered when rapid spin rotations are applied. This suggests the short range spatial modulations of the condensate have been suppressed by nullifying the dipolar effects.

Appendix C

Deriving the Density of States

For the 2D periodic boundary system only certain waves are allowed that satisfy the boundary conditions. The width of the box must contain an integer number of half wavelengths, meaning the possible wavelengths along each axis are given by,

$$\lambda_\nu = 2w, w, \frac{2w}{3}, ..., \frac{2w}{n_{\lambda_\nu}}, \quad \nu = x, z, \quad n_{\lambda_\nu} = 1, 2, ... \tag{C.1}$$

where w is the width of the system and n_{λ_ν} is the number state attributed to the wave. The possible momentums, $k = 2\pi/\lambda$ are then,

$$k_\nu = \frac{\pi}{w}, \frac{2\pi}{w}, \frac{3\pi}{w}, ..., \frac{n_{\lambda_\nu}\pi}{w} \tag{C.2}$$

All the possible momentum modes can then be represented by a point in momentum space. As shown graphically in Figure C.1. The total number of momentum states, G, with less momentum than k can then be approximated by calculating the momentum space area enclosed by the quarter circle of radius k and dividing by the momentum space area between four adjacent points, $a_k = w^2/\pi^2$. This gives,

$$G(k) = \frac{w^2 k^2}{4\pi}. \tag{C.3}$$

The kinetic energy of a state, $\epsilon_k = k^2/2$, can then be substituted in for k to give the total number of states up to a certain kinetic energy,

$$G(\epsilon_k) = \frac{w^2 \epsilon_k}{2\pi}. \tag{C.4}$$

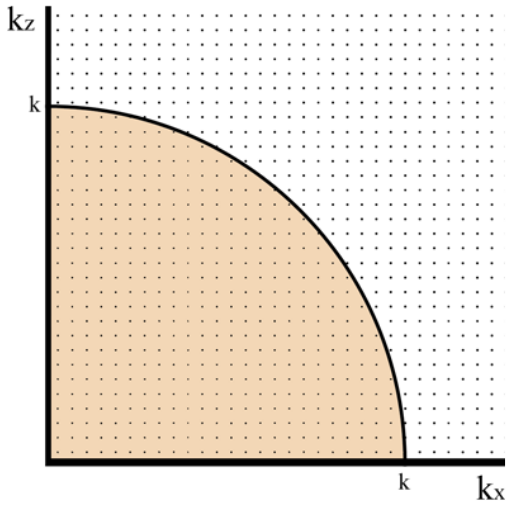

Figure C.1: The momentum space representation of the density of states. Each point represents a possible pair of k-values relating to an allowed wave through the system. The area of a square with four adjacent points as its corners is given by w^2/π^2. The total number of states with a magnitude of momentum less than k can be approximated by the area of the quarter circle divided by the area of the individual squares.

The density of states, g, for the system is then given by the derivative of the total number with respect to ϵ_k,

$$g(\epsilon_k) = \frac{w^2}{2\pi}, \tag{C.5}$$

this is the number of states per unit energy in the two dimensional system.